R. & M. No. 2559
(8581, 9946, 9882)
A.R.C. Technical Report

MINISTRY OF SUPPLY

AERONAUTICAL RESEARCH COUNCIL

REPORTS AND MEMORANDA

Influence of Tuned Dampers on Flexure-Aileron Flutter

Part I

Theoretical Investigation on the Influence of Tuned Damping Devices on Flexure-Aileron Flutter

By

R. A. FRAZER, B.A., D.Sc., and W. P. JONES, M.A.

Part II

Some Further Calculations on the Influence of Tuned Damping Devices on Flexure-Aileron Flutter

By

W. P. JONES, M.A.

Part III

Experiments on the Effect of Tuned Damping Devices on Flexure-Aileron Flutter

By

C. SCRUTON, B.Sc., D. V. DUNSDON, and P. M. RAY, B.A.

LONDON: HER MAJESTY'S STATIONERY OFFICE

1952

PRICE 8s 6d NET

Influence of Tuned Dampers on Flexure-Aileron Flutter

Part I

Theoretical Investigation on the Influence of Tuned Damping Devices on Flexure-Aileron Flutter

By

R. A. FRAZER, B.A., D.Sc., and W. P. JONES, M.A.,
of the Aerodynamics Division, N.P.L.

Reports and Memoranda No. 2559*

20*th September*, 1946

General Summary.—In Part I a general theory has been developed for the investigation of the influence of damping devices of various types on flexure-aileron flutter. The numerical applications refer to a large transport aircraft, and they are restricted to the case of a mass-balanced aileron-carried damper. From the diagrams given at the end of the Part it is inferred that this type of damper would be unsatisfactory as a flutter preventive.

Part II supplements Part I and gives results for a partly balanced and for a completely balanced aileron-damper system. It is concluded that tuned dampers of these types would also prove unreliable.

Part III describes an experimental investigation into the effect on flexure-aileron flutter of a tuned damping device attached to the aileron. The results confirm the theoretical conclusion that the use of an aileron-carried damper would not be a reliable flutter preventive.

1. *Introduction.*—In the present report a general theoretical method is given for the investigation of the influence of damping devices of various types on flexure-aileron flutter.

The numerical applications refer to a large transport aircraft, and are restricted to simple aileron-carried dampers—namely, to dampers with a casing which is spring-connected to the aileron or its control system, but not spring-connected to the wing itself.

A direct prediction of the flutter characteristics, for a specific damper, would present considerable difficulties and provide only limited information. The method actually used is inverse in the sense that the critical speed and frequency are treated as assigned, and the appropriate 'critical relations' connecting the damper constants are deduced. The results so obtained can be presented as curves, and cross-plotting yields final diagrams showing how the critical speed varies with the amount of the artificial damping and with the natural frequency of the damper.

The method requires the use of three types of diagram. These are described in section 3, and are referred to as: (i) the (x, y) diagram, (ii) the intermediate diagram, (iii) the final damping diagram. Examples of all these diagrams appear at the end of the report.

2. *Outline of General Theory.*—Fig. 1 is a diagram of the most general system considered. For simplicity, the damper is represented as a symmetrical cylindrical casing C capable of rotation about the aileron hinge axis and supporting (in the most general case) an out-of-balance mass M.

* Published with the permission of the Director, National Physical Laboratory.

A spring σ and constant artificial damping μ are provided between the casing and the aileron, and a spring connection Σ can also be present between the casing and the wing. It is convenient to write

$$In^2 = \sigma + \Sigma\,; \; IN^2 = \Sigma\,. \qquad \ldots \quad \ldots \quad \ldots \quad \ldots \quad (2.1)$$

Thus $n/2\pi$ denotes the natural frequency of the *undamped* casing, with the wing and aileron assumed to be rigidly held, while N denotes the corresponding natural frequency when the spring σ is removed.

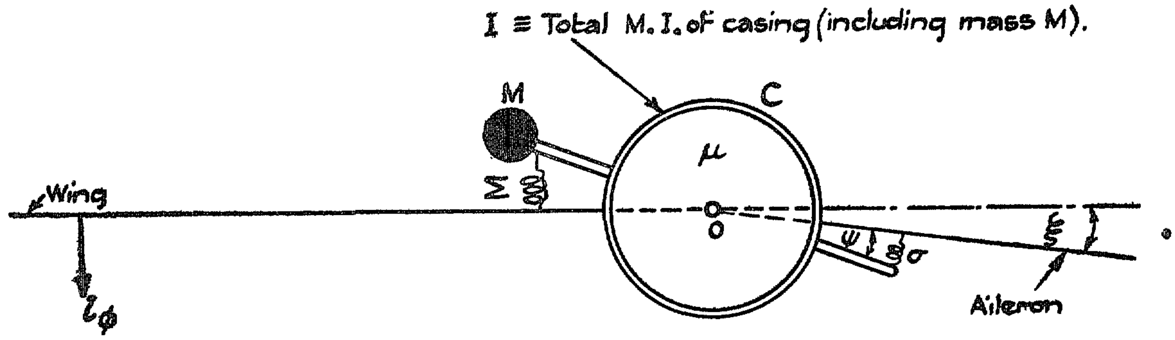

FIG. 1. Diagram of flexure-aileron system.

The damper will be said to be aileron-carried when $\Sigma = 0$, wing-carried when $\sigma = 0$, and wing-aileron carried when both springs are present. Moreover, when $M = 0$, the damper will be described as mass-balanced. The binary system obtained when the damper and the springs are completely removed will be referred to, for brevity, as the parent system. The practical equivalent of a balanced aileron-carried damper would be a damping device placed within the wing but spring-mounted on the aileron operating rod. When M is present and $\Sigma = 0$, the system is effectively a damped flexible-aileron mass-balancing device.

Table 1 defines the non-dimensional dynamical coefficients, which are for simplicity assumed to be independent of the frequency parameter. Appropriate non-dimensional equivalents for the elastic stiffnesses and the artificial damping are introduced later. The coefficients A_1, P, D_2 denote the total inertias (structural plus aerodynamic) for the parent system, while $-\tilde{\omega}$ and I represent respectively the effective additions to the product of inertia and the aileron moment of inertia due to the damper casing. Thus, when M lies forward of the aileron hinge axis, as shown in Fig. 1, $\tilde{\omega} > 0$. The addition to A_1 due to the damper casing and balancing mass M is neglected throughout.

TABLE 1

*Dynamical Coefficients**

Wing Flexural Moments (ϕ)		Hinge Moments (ξ)		Damper Moments (ψ)	
Symbol	Equivalent	Symbol	Equivalent	Symbol	Equivalent
A_1	$\rho l^3 c_0^2 a_1$	$P - \tilde{\omega}$	$\rho l^2 c_0^3 (P_0 - \tilde{\omega}_0)$	$-\tilde{\omega}$	$-\rho l^2 c_0^3 \tilde{\omega}_0$
B_1	$\rho V l^3 c_0 b_1$	B_2	$\rho V l^2 c_0^2 b_2$	—	—
$C_1 + l_\phi$	$\rho V^2 l^3 c_1 + l_\phi$	C_2	$\rho V^2 l^2 c_0 c_2$	—	—
$P - \tilde{\omega}$	$\rho l^2 c_0^3 (P_0 - \tilde{\omega}_0)$	$D_2 + I$	$\rho l c_0^4 (d_2 + I_0)$	I	$\rho l c_0^4 I_0$
E_1	$\rho V l^2 c_0^2 e_1$	E_2	$\rho V l c_0^3 e_2$	—	—
F_1	$\rho V^2 l^2 c_0 f_1$	$F_2 + h_\xi + \Sigma$	$\rho V^2 l c_0^2 f_2 + h_\xi + \Sigma$	Σ	Σ
$-\tilde{\omega}$	$-\rho l^2 c_0^3 \tilde{\omega}_0$	I	$\rho l c_0^4 I_0$	I	$\rho l c_0^4 I_0$
—	—	—	—	μ	μ
—	—	Σ	Σ	$\sigma + \Sigma$	$\sigma + \Sigma$

* Reference section is at $y = l$, and root chord is c_0.

It is assumed that the damper constants are such that steady oscillations of the complete system, having frequency $f \equiv p/2\pi$, occur at airspeed V. The following additional symbols are required*.

$$\left.\begin{aligned}
\Omega &\equiv V/pc_0 \text{ (reciprocal of frequency parameter)}\,,\\
\alpha &\equiv X + ib_1\Omega + c_1\Omega^2, \text{ where } X \equiv -a_1 + (l_\phi/\rho l^3 c_0{}^2 p^2)\,,\\
\beta &\equiv -P_0 + ie_1\Omega + f_1\Omega^2\,,\\
\gamma &\equiv -P_0 + ib_2\Omega + c_2\Omega^2\,,\\
\delta &\equiv Y + ie_2\Omega + f_2\Omega^2, \text{ where } Y \equiv -d_2 + (h_\xi/\rho l c_0{}^4 p^2)\,,\\
K &\equiv I_0\left(1 - \frac{N^2}{p^2}\right),\\
k &\equiv I_0\left(\frac{n^2}{p^2} - 1\right),\\
\mu &= \rho l c_0{}^4 p \mu_0\,.
\end{aligned}\right\} \qquad \ldots \quad \ldots \quad (2.2)$$

Then if $\bar{\phi}$, $(l/c_0)\bar{\xi}$, $(l/c_0)\bar{\varphi}$ denote the respective complex amplitudes, the conditions for steady oscillations can be expressed as

$$\left.\begin{aligned}
\alpha\bar{\phi} + (\beta + \tilde{\omega}_0)\bar{\xi} + \tilde{\omega}_0\bar{\varphi} &= 0\,,\\
(\gamma + \tilde{\omega}_0)\bar{\phi} + (\delta - K)\bar{\xi} - K\bar{\varphi} &= 0\,,\\
\tilde{\omega}_0\bar{\phi} - K\bar{\xi} + (k + i\mu_0)\bar{\varphi} &= 0\,.
\end{aligned}\right\} \ldots \quad \ldots \quad \ldots \quad \ldots \quad (2.3)$$

These yield the two relations

$$(k + i\mu_0)(x - K - iy) = E + iF\,. \quad \ldots \quad \ldots \quad \ldots \quad (2.4)$$

$$\frac{\bar{\varphi}}{\bar{\xi}} = \frac{\alpha(x - K - iy)}{\tilde{\omega}_0(\gamma + \tilde{\omega}_0) + \alpha K}\,, \quad \ldots \quad \ldots \quad \ldots \quad \ldots \quad (2.5)$$

where

$$\alpha(x - iy) \equiv \begin{vmatrix} \alpha & \beta + \tilde{\omega}_0 \\ \gamma + \tilde{\omega}_0 & \delta \end{vmatrix}\,, \quad \ldots \quad \ldots \quad \ldots \quad (2.6)$$

$$\alpha(E + iF) \equiv \alpha K^2 + (\beta + \gamma)K\tilde{\omega}_0 + (K + \delta)\tilde{\omega}_0{}^2\,. \quad \ldots \quad (2.7)$$

Equation (2.6) can be written alternatively

$$\begin{vmatrix} \alpha & \beta + \tilde{\omega}_0 \\ \gamma + \tilde{\omega}_0 & \delta - x + iy \end{vmatrix} = 0\,. \quad \ldots \quad \ldots \quad (2.6\text{ bis})$$

A direct prediction of the critical speeds by (2.4) for a given set of damper constants would involve great complication. An inverse treatment, based on the use of the diagrams described in section 3, appears to be preferable.

3. *General Description of Diagrams.*—For numerical work use is made of three types of diagram.

(i) *The (x, y) Diagram.*—To construct this, $\tilde{\omega}_0$ and ρ are treated as known, the values of α, β, γ, δ are tabulated against p for constant values of V, and the results are plotted as curves $V =$ const. and $p =$ const. in the plane of (x, y)†. The diagram so obtained is applicable for all dampers with a given product of inertia $\tilde{\omega}_0$, and for a given air density.

* The symbol i denotes throughout the imaginary unit $\sqrt{-1}$.

† Alternatively curves $V =$ const. are plotted in the planes of (x, y) and of (x, p).

Examples of (x, y) diagrams, appropriate to balanced aileron-carried dampers, are given in Figs. 3 and 7; for such dampers only the upper half of the diagram, corresponding to $y > 0$ $(\mu > 0)$, is required. The curves $V =$ const. in these cases consist of simple (non-circular) arcs standing on OX, which grow and move towards the right as V is increased. The first member, corresponding to a certain lower speed bound (about 90 ft/sec for Fig. 3), just contacts Ox, and thus consists effectively of two coincident points. When V reaches a specific value (about 850 for Fig. 3) the right-hand extremity of the curve becomes asymptotic to Ox: the asymptote remains horizontal, but moves upwards, when V is further increased.

It is to be noted that although any given pair of *real* positive values (V, p) lead to a unique point $Q(x, y)$ in the diagram, the converse is not in general true. A given point Q usually corresponds to two distinct values (V, p); moreover, only a limited region of the (x, y) plane corresponds to real positive values (V, p).

From (2.6 bis) it follows that the (V, p) values corresponding to any point $Q(x, 0)$ lying on Ox are given by the critical speeds and frequencies for the parent system with d_2 increased by x and P_0 reduced by $\tilde{\omega}_0$.

(ii) *The Intermediate Diagram.*—This consists of curves $(\mu, 1/n)$ corresponding to constant values of V, and is obtained with the help of the (x, y) diagram, once I_0 and N are assigned. Equations (2.4) and (2.7) can be used to calculate μ_0 and k, and so the values of μ and n.

The diagram usually presents complicated features, and the curves are often apt to depend sensitively on variations of V and p. Examples are provided by Figs. 4 and 8. The construction of the curves can often be aided by a judicious geometrical interpretation of the (x, y) diagram (*see* section 4).

An additional intermediate diagram (*e.g.* curves (μ, p) for $V =$ const.) may be required, if values of the amplitude ratio (2.5) have to be determined.

(iii) *The Final Damping Diagram.*—This is obtained directly from (ii) by cross-plotting, and yields the required curves $(V, 1/n)$ corresponding to constant values of μ (compare, for instance, Figs. 5, 6 and 9).

4. *Balanced Aileron-carried Dampers.*—When $M = 0$ and $\Sigma = 0$ (*i.e.*, when $\tilde{\omega}_0 = 0$, $N = 0$, $K = I_0$) equations (2.4) and (2.7) reduce to

$$x - iy = \delta - \frac{\beta\gamma}{\alpha}\,, \qquad (4.1)$$

$$\frac{n^2}{p^2} = \frac{x^2 + y^2 - I_0 x}{(x - I_0)^2 + y^2}\,, \qquad (4.2)$$

$$\frac{\mu}{\rho l c_0{}^4 p} = \frac{I_0{}^2 y}{(x - I_0)^2 + y^2}\,. \qquad (4.3)$$

Also

$$I_0{}^2 r^2 = (x - I_0)^2 + y^2\,, \qquad (4.4)$$

where r denotes the true damper-aileron amplitude ratio $|\psi|/|\xi|$.

Equations (4.2) and (4.3) can be interpreted geometrically as shown in Fig. 2. By (4.3) it is seen that only the upper half of the (x, y) diagram, corresponding to $y > 0$ $(\mu > 0)$, is of practical interest in relation to aileron-carried dampers. The semi-circles passing through A and orthogonal to Ox correspond to constant values of n/p; while the full circles, corresponding to $\mu/p =$ const., touch Ox at A. The two loci $n/p = 1$ and $\mu/p = 0$ are, of course, to be regarded as circles of infinitely large radii.

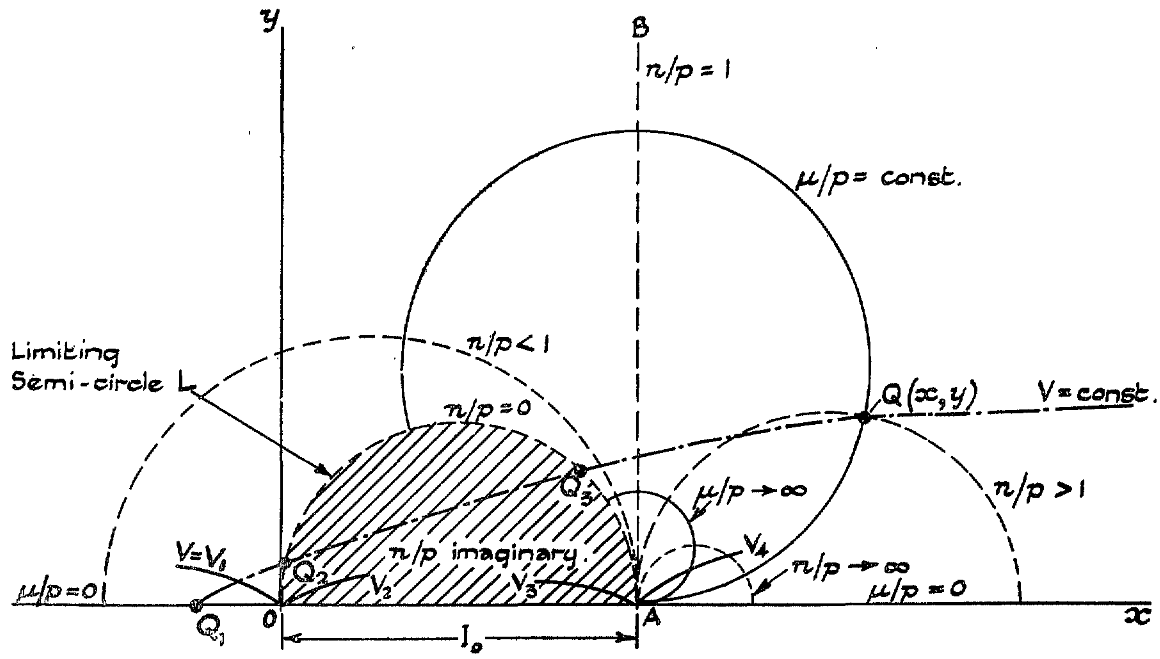

FIG. 2. Detail of (x, y) diagram for balanced aileron-carried damper.

Fig. 2 gives useful guidance in the construction of the intermediate and the final damping diagrams, particularly as regards the number and the positioning of curved branches and asymptotes. For example, it is at once seen from Fig. 2 that any curve V = const. which cuts the limiting semi-circle L in two real points must give rise to a curve $(\mu, 1/n)$ in the *intermediate* diagram which consists of two distinct branches. The first branch, derived from the left-hand arc $Q_1 Q_2$ in Fig. 2, will start with a zero ordinate $\mu = 0$ (Q at Q_1), and end with a horizontal asymptote $1/n \rightarrow \infty$ (Q at Q_2). The second branch will be similar, and have a horizontal asymptote when Q lies at Q_3, and a zero ordinate when Q is at the right-hand intersection of V = const. with Ox*. In other cases only one branch, or no branch at all, may appear in the intermediate diagram.

The interpretation of Fig. 2 calls for care when a curve V = const. closely approaches the point A. The two distinct pairs of values of V and p, say (V_3, p_3) and (V_4, p_4), appropriate to the point A are given by the critical speeds and frequencies of the binary parent system with its aileron inertia d_2 increased by I_0†. The damper can then be regarded as effectively locked to the aileron, either due to infinite stiffness $\sigma (1/n \rightarrow 0)$ in conjunction with arbitrary damping μ, or due to infinite damping in conjunction with arbitrary σ or $1/n$. It follows that, in the intermediate diagram, the homologue of the point A will consist of the axis $1/n = 0$ together with the line $\mu = \infty$, and that these two components will form part of the loci corresponding to $V = V_3$ and $V = V_4$‡.

An inspection of Fig. 2 will make clear the changes as Q closely approaches the singularity A. If the point B is regarded as due North of A, these changes can be summarized as follows.

Direction of approach of Q towards A	$1/n$	μ
From due East (*i.e.*, along xA)	$\rightarrow 0$	0
Easterly (but not along xA)	$\rightarrow 0$	finite ($\neq 0$)
North-easterly	$\rightarrow 0$	$\rightarrow \infty$
Northerly, or from due North.. ..	finite	$\rightarrow \infty$
Along limiting semi-circle	∞	$\rightarrow \infty$

* The second intersection (not shown in Fig. 2) exists unless V is very large. An illustration of the case discussed is provided by the curve for $V = 140$ in Fig. 3.

† *See* end of section 3 (i).

‡ *See* for example curves for $V = 149$ and 183 in Fig. 3.

It may be noted, finally, that the origin 0 in the (x, y) diagram corresponds to the critical speeds and frequencies, say (V_1, p_1) and (V_2, p_2), of the binary parent system. Then $\mu = 0$ and $1/n \rightarrow \infty$, so that the locus corresponding to $V = V_1$ in the intermediate diagram will be asymptotic to the axis $\mu = 0$. The locus corresponding to $V = V_2$ will also by asymptotic to $\mu = 0$, but will approach this axis from below and thus not appear in the actual diagram $(\mu > 0)$. However, it will possess a second branch if the curve $V = V_2$ in Fig. 2 extends beyond A.

5. *Numerical Data.*—The diagrams summarized in section 6 all refer to a large transport aircraft (wing semi-span $s = 105$ ft, root chord $c_0 = 30 \cdot 35$ ft, $l = 78 \cdot 75$ ft). Wind tunnel experiments on the flexure-aileron flutter of the wing, and tests of the influence of 'plain' artificial aileron damping (casing locked to the wing), have been carried out by Scruton[1] (1944). Critical speeds for the wing have also been predicted by Jones[2] (1944).

For the present calculations the inertial coefficients adopted correspond to those given by Scruton in Fig. 4 of R. & M. 2480[1]. The values are tabulated below.

*Inertial Coefficients**

Linear mode in flexure

Inertia	Structural	Aerodynamic	Total	
			$h = 0$ ($\varrho_0 = 0 \cdot 002378$)	$h = 30{,}000$ ft ($\varrho_0/\varrho = 2 \cdot 672$)
Flexural Moment	$\bar{a}_1 = 1 \cdot 836$ (5·966)	$\hat{a}_1 = 0 \cdot 224$	$a_1 = 2 \cdot 06$ (6·19)	$a_1 = 5 \cdot 13$
Product	$\bar{P}_0 = 0 \cdot 00133$	$\hat{P}_0 = 0 \cdot 0007$	$P_0 = 0 \cdot 00203$	$P_0 = 0 \cdot 00425$
Aileron Moment ..	$\bar{d}_0 = 0 \cdot 000276$	$\hat{d}_2 = 0 \cdot 000019$	$d_2 = 0 \cdot 000295$	$d_2 = 0 \cdot 000756$

The flexural stiffness $l_\phi = 1 \cdot 892 \times 10^8$ lb ft/rad was kept constant throughout, and the value $h_\xi = 8{,}000$ lb ft/rad was assumed for the aileron control stiffness in the symmetrical flutter calculations. For anti-symmetrical flutter $h_\xi = 0$. When the fuel tank was empty the natural frequency in flexure was $f = 1 \cdot 475$, which gave $p_n = 2\pi f = 9 \cdot 266$. For the tank-full case $f = 0 \cdot 8507$ and $p_n = 5 \cdot 345$.

The critical speeds for anti-symmetrical flutter deduced by Scruton for full-scale from the model tests were 121 and 169 ft/sec for tank empty and flight at sea level. Calculations, based on a set of frequency-independent derivatives derived from the two-dimensional vortex strip theory in R. & M. 2362[2] for $\omega = 2 \cdot 0$, led to considerably lower critical speeds (98 and 117 ft/sec). However, more recent experimental results obtained by Scruton[3] indicated that a factor $0 \cdot 6$ should be applied to the theoretical values of e_2 and f_2, and in the light of this evidence the same factor was adopted for f_1 and b_2, although the full theoretical value was retained for b_1. For simplicity it was also assumed that $c_1 = c_2 = 0$. The final set of coefficients used was as follows.

$$b_1 = 0 \cdot 833, \quad e_1 = 0 \cdot 00081, \quad b_2 = 0 \cdot 0004944, \quad e_2 = 0 \cdot 0003672,$$

$$c_1 = 0 \quad , \quad f_1 = 0 \cdot 168 \quad , \quad c_2 = 0 \quad , \quad f_2 = 0 \cdot 001326 \quad .$$

The predicted critical speeds (123 and 149 ft/sec) were then in better agreement with those determined experimentally.

* Figures in brackets correspond to the tank-full case.

Most of the damping diagrams given relate to anti-symmetrical flutter; for the symmetrical case, the value $h_\xi = 8{,}000$ lb ft/rad was adopted for full scale.

Two values were taken for the moment of inertia coefficient of the damper casing, namely,

$$I_2 = 0 \cdot 1 d_2 = 0 \cdot 1069 \bar{d}_2 ,$$

and

$$I_2 = 0 \cdot 5 d_2 = 0 \cdot 5344 \bar{d}_2 .$$

The coefficient $\bar{d}_2$ corresponds to an actual structural aileron moment of inertia of $\bar{D}_2 = 43 \cdot 85$ slug ft^2 for full-scale. The two values taken for I were accordingly

$$I = 4 \cdot 688 \text{ slug ft}^2$$

and

$$I = 23 \cdot 43 \text{ slug ft}^2 .$$

6. *Summary of Illustrative Diagrams.*—The diagrams, which do not lend themselves to detailed discussion, are listed below. They all refer to the full-scale aircraft, and—with the exception of Fig. 16—to balanced aileron-carried dampers.

Main Diagrams

Figure Number	Type of Flutter*	h (ft)	$I/\bar{D}_2$	Tank	Description
3	A	0	—	empty	(x, y)
4	,,	0	0·5344	,,	intermediate
5	,,	0	0·5344	,,	final damping
6	,,	0	0·1069	,,	,, ,,
7	A	30,000	—	empty	(x, y)
8	,,	30,000	0·1069	,,	intermediate
9	,,	30,000	0·1069	,,	final damping
10	A	0	0·1069	full	final damping
11	S	0	—	empty	(x, y)
12	,,	0	0·1069	,,	intermediate
13	,,	0	0·1069	,,	final damping

Supplementary Diagrams (Antisymmetrical Flutter and Tank Empty)

Figure Number	Description
14	Critical speeds and frequencies with casing locked to aileron ($h = 0$)
15	Critical speeds and frequencies with casing locked to aileron ($h = 30{,}000$)
16	Influence of plain artificial damping with casing locked to wing ($h = 0$ and $h = 30{,}000$ ft)
17	Amplitude ratio for case of Fig. 9.

* A denotes ' antisymmetric ' and S denotes ' symmetric '.

7. *General Conclusions*.—For the particular aircraft considered antisymmetrical flutter of the parent system occurs at low speeds, but symmetrical flutter is absent. Prevention of the antisymmetrical flutter by the use of a mass-balanced aileron-carried tuned damper would, however, involve considerable risk due to

(i) the difficulty of deciding on the tuning frequency and the amount of damping beforehand (*see* Figs. 6, 9 and 10);

(ii) the danger of flutter due to any large accidental increase of damping (*e.g.*, freezing of oil or jamming). The effect of the damper would then be represented by an increase in the aileron moment of inertia which would result in a slight increase of critical speed (*see* Figs. 6 and 14);

(iii) symmetrical flutter resulting from too low a value of the damping (*see* Fig. 13);

(iv) altitude effects (at $h = 30{,}000$ ft, flutter occurs for all values of μ and $1/n$, *see* Figs. 6 and 9).

In view of the above objections, it appears that a mass-balanced aileron-carried tuned damper would not be a reliable flutter preventive.

Acknowledgment.—The authors wish to acknowledge the help given in this investigation by Miss Sylvia W. Skan and Mrs. J. M. Muir, who did most of the numerical work.

Part II

Some Further Calculations on the Influence of Tuned Damping Devices on Flexure-Aileron Flutter

By

W. P. Jones, M.A.,

of the Aerodynamics Division, N.P.L.

8. In Part I of this report the effect of tuned aileron-carried dampers* on flexural-aileron flutter was considered. The damper was assumed to be balanced, but the aileron-damper system as a whole was unbalanced. In the present note results for a partly balanced and for a completely balanced aileron-damper system are given. Most of the calculations are based on a larger value of the product of inertia than that used in the original calculations. Only antisymmetrical flutter ($h\xi = 0$) is considered, and, in the notation of Part I, the inertia I of the casing (including the out-of-balance mass M) is maintained constant at the value

$$I = 0 \cdot 1069 \bar{D}_2 = 4 \cdot 688 \text{ slug ft}^2.$$

The cases considered are listed in the following table:—

TABLE 2

Product of Inertia Values for Cases Considered

Units:—slug, foot.

Aileron	h	$\bar{P}$ (structural)	P (total)	$\tilde{\omega}$	Figure	Condition of Aileron-damper System
Original	0	547	835	835	18	Balanced at sea level†.
	30,000	547	655	835	19	,, ,, ,, ,,
Heavier Aileron . .	0	1382	1670	0	20	Balanced damper only.
	30,000	1382	1490	0	21	,, ,, ,,
	Plain artificial damping				22	Casing locked to wing.
	0	1382	1670	835	23	Partly balanced aileron.
	30,000	1382	1490	835	24	,, ,, ,,
	0	1382	1670	1670	25	Balanced at sea-level.
	30,000	1382	1490	1670	26	,, ,, ,, ,,

† The aileron-damper system is said to be balanced when $P - \tilde{\omega} = 0$.

The diagrams show that a tuned damper may produce flutter even when the aileron-damper system is mass-balanced if the damping μ has too low a value. For the partly mass-balanced system, it would be possible to prevent flutter at $h = 0$ by a proper choice of μ and $1/n$, but flutter would probably occur at a higher altitude (*see* Figs. 23 and 24). These results confirm the conclusion drawn in Part I that a tuned damper would not make a reliable flutter preventive.

* *See* Fig. 1 of Part I.

Part III

Experiments on the Effect of Tuned Damping Devices on Wing Flexure-Aileron Flutter

By

C. SCRUTON, B.Sc., MISS D. V. DUNSDON, and P. M. RAY, B.A.,

of the Aerodynamics Division, N.P.L.

---

9. *Introduction.—Range and Purpose of the Investigation.*—R. & M. 2480[1] describes tests on the effect on flexure-aileron flutter of artificial damping applied directly to the aileron by a damper carried in the wing. The amount of damping for flutter prevention indicated by these experiments could probably be supplied by dampers of small mass as compared with the balance mass which the dampers replace, but the damping forces to be overcome during normal operation of the control column would be too great. A tuned damping device attached to the control surface which would normally offer little resistance to movements of the control was suggested as a possible alternative. A theoretical investigation by Frazer and Jones on the effect of tuned dampers is described in Parts I and II of this report. Part III describes a parallel experimental investigation.

A balanced aileron-carried damper was tested under conditions corresponding to zero altitude, and to an altitude of 30,000 ft: a few tests on an unbalanced aileron-carried damper were also made.

10. *Description of the Model.*—

(*a*) *Degrees of Freedom.*—

(i) Wing flexure with linear mode of displacement from the wing root.

(ii) Aileron angular movement about the hinge line.

(iii) Angular movement of the damper disc* about an axis coincident with the aileron hinge axis.

(*b*) *Scales.*—The linear and speed scales of the model were chosen to be $1/20$ and $1/\sqrt{20}$ of full-scale respectively. Hence the scales for moments and products of inertia, frequencies, elastic stiffness (moment per radian) and damping coefficients (moment per radian per second) were respectively $1/20^5$, $\sqrt{20}$, $1/20^4$ and $1/20^4\sqrt{20}$.

(*c*) *Construction of the Model.*—The plan form and the full-scale dimensions of the wing are shown in Fig. 27.

The model wing was a light rigid structure with plan form and section similar to that proposed for B.A.C. aircraft type 167 but without camber. It was attached at its root to a mock fuselage by ball bearings which permitted wing flexural movement only. The mock fuselage was fixed to the tunnel wall and the wing was supported in a horizontal position by the helical springs which provided the flexural stiffness.

The rigid aileron, with the damper casing fixed to its inboard end, was attached to the wing by two small ball bearings. From the outboard tip of the aileron a balance arm, which was also used for the attachment of aileron stiffness springs, projected into a cut-out in the wing. The aileron section had straight sides and a D-nose which fitted closely into the shroud (Fig. 28).

---

* The damper disc corresponds to the damper casing of Part I.

The arrangement of the tuned damper is shown in Fig. 29. The brass disc A was enclosed by the damper casing B and was carried by a spindle supported on two small ball bearings fitted to the damper casing. One end of the spindle projected outside the casing and carried a fitting C to which one end of a spiral spring was clamped. The other end of the spiral spring was clamped to the outside of the casing by fitting D. The casing was provided with filler and drainage plugs to enable various damping fluids to be introduced into the casing. Thus the disc rotated relative to the casing about an axis coincident with the aileron hinge axis; the motion being resisted by the elastic forces of the spiral spring and by the damping forces due to the fluid. The spiral springs used were made from steel wire of various diameters and were wound with either 1 or $1\frac{1}{2}$ complete turns. The inertial values of the disc could be varied by balance masses placed on two small arms attached to the fitting C.

When the balance masses were symmetrically placed about the rotation axis the device corresponded to the mass-balanced aileron-carried damper as defined in Part I.

11. *Definition of Symbols.*

ξ	Aileron angle
ψ	Damper disc angular displacement relative to aileron
ϕ	Wing displacement in flexure
$^*I_{\phi\phi}$	Moment of inertia of wing, including aileron, about wing root as measured in still air at $h = 0$
$^*I_{\xi\xi}$	Moment of inertia of aileron excluding damper disc about the hinge line as measured in still air at $h = 0$
$I_{\psi\psi}$	Polar moment of inertia of damping disc and associated balance masses, including the virtual mass effect of the damping fluid
$I_{\phi\xi}$	Product of inertia of aileron excluding the damper disc with respect to the aileron hinge axis and the wing root, as measured in still air at $h = 0$
$I_{\psi\phi}$	Product of inertia of damping disc with respect to the disc axis and the wing root
l_ϕ	Elastic stiffness of wing in flexure expressed as moment per radian
$f_\phi{}^*$	Natural frequency of wing in flexure
l_ξ	Elastic stiffness of aileron expressed as the aileron hinge moment per radian deflection
l_ψ	Elastic stiffness of damper disc expressed as moment per radian
μ	Artificial damping coefficient between damper disc and casing expressed in moment per radian per second. The values quoted are those obtained from forced oscillation experiments on the disc with the casing stationary
n^*	$2\pi \times$ natural frequency of the undamped disc
h	Altitude
V_c, f_c,	Critical speed and frequency respectively for the onset of flutter (lower critical speed and frequency)
$\bar{V}_c$, $\bar{f}_c$	Critical speed and frequency at which the existing flutter is suppressed (upper critical speed and frequency)

12. *Method of Test.*—The lowest value of μ was obtained with the damper casing empty; higher values were obtained by filling the damper casing with oils of various viscosities. The oils used ranged from light machine oil to heavy gear oil. For each value of μ, critical speeds and

* These symbols are barred when they refer to the effective values at the upper critical speed (*See* section 12).

frequencies were measured in the usual way for a range of values of n obtained by changing the damper spring. To keep the value of $I_{\psi\psi}$ constant it was necessary to correct for the difference between the virtual moment of inertia of the disc when immersed in oil and in air. This correction was made by adjustment of the balance masses on the disc arms. A measure of the value of μ for each oil was obtained by a forced oscillation experiment on the disc while the casing was held stationary. When applied to the flutter tests this value must be regarded as qualitative, since it may not be truly applicable to the conditions obtaining in flutter, when both disc and casing rotate. Since the value of μ was found to be dependent on frequency, μ was always measured at a frequency close to the flutter frequency. The value of n was calculated from the measured values of $I_{\psi\psi}$ and l_{ψ}.

In order to correlate the experiments with the theoertical work of Parts I and II, the effective model inertial and stiffness coefficients were adjusted to correspond approximately to those assumed in the theoretical work. For tests applicable to zero altitude the actual model values of $I_{\phi\phi}$ and $I_{\xi\xi}$ were too high, and recourse was made to additions to the elastic stiffnesses to obtain effectively the required inertial values. The effective value of $I_{\xi\xi}$ for antisymmetrical flutter ($l_{\xi} = 0$) and the effective value of $I_{\phi\phi}$ associated with a wing flexural stiffness l_{ϕ} are given respectively by the following relations.

$$I_{\xi\xi} = {}_TI_{\xi\xi} - \frac{{}_Tl_{\xi}}{4\pi^2 f^2} ,$$

$$I_{\phi\phi} = {}_TI_{\phi\phi} - \frac{({}_Tl_{\phi} - l_{\phi})}{4\pi^2 f^2} ,$$

where symbols with the prefix T refer to test values and f is the flutter frequency. Due to the slight difference between f_c and $\bar{f}_c$ the values of $I_{\xi\xi}$ and $I_{\phi\phi}$ corresponding to V_c and $\bar{V}_c$ differed by about 5 per cent.

The effect of altitude was simulated on the model by increasing the non-aerodynamic coefficients (inertia, damping, stiffness) by ρ_0/ρ_h where ρ_0, ρ_h are respectively the air densities at the altitude of the test and at altitude h. It was not practicable to increase the moment of inertia of the damper disc to the desired value but the results were referred to the desired effective value of $I_{\psi\psi}$ associated with an effective stiffness given by

$$l_{\psi} = {}_Tl_{\psi} - 4\pi^2 f^2 ({}_TI_{\psi\psi} - I_{\phi\phi}) .$$

The effect of the difference between $\bar{f}_c$ and f_c was to give different values of $I_{\psi\psi}$, and hence different values of n corresponding to the lower and upper critical speeds.

13. *Results*.—All values quoted refer to the full-scale aircraft and are expressed in slug-foot-second units.

(a) $h = 0$, *balanced damper*.—The results are given in Table 3. Curves of critical speed against $1/n$ for constant values of μ are plotted in Fig. 30. For a small range of the disc natural frequency near the natural frequency of the wing in flexure flutter was prevented for values of $\mu < 51$. This range was narrower than that predicted theoretically (*see* Fig. 6) and did not show much variation with μ. For $\mu = 71$ and over flutter occurred for all natural frequencies of the damper disc.

(b) $h = 30{,}000$ *ft, balanced damper*.—The results are given in Table 4 and are plotted in Fig. 31. Flutter occurred for all the variations of n and μ tested. A small increase in V_c was found when the natural frequencies of the damper disc and of the wing in flexure were nearly equal. These experimental results agree qualitatively with the theoretical results plotted on Fig. 9.

(c) $h = 0$, *unbalanced damper* (*Table* 5, *Fig.* 32).—For these tests mass was placed on the disc arm forward of the axis. The mass used was not quite sufficient to eliminate flutter when the damper disc was locked to the aileron, and flutter occurred over a small range of wind speed. With the damper disc spring constrained to the aileron, flutter was not obtained for any finite value of μ tested when n was greater than $2\pi f_\phi$, but was present over a wide range of wind speed for certain values of n less than $2\pi f_\phi$.

14. *Conclusion.*—The experiments provide qualitative confirmation of the theoretical results given in Parts I and II, and support the conclusion that the use of an aileron-carried damper would not be a reliable flutter preventive.

TABLE 3

Results for Antisymmetrical Flutter with a Balanced Aileron-carried Damper—Zero Altitude

General Conditions

(a) Stiffnesses $l_\xi = 0$,
$l_\phi = 1\cdot 892 \times 10^8$.

(b) Inertias $I_{\psi\psi} = 5\cdot 73,\ I_{\psi\phi} = 0$,
$I_{\xi\xi} = 44\cdot 8\ (I_{\psi\psi} = 0\cdot 128\, I_{\xi\xi})$,
$\bar{I}_{\xi\xi} = 48\cdot 1\ (I_{\psi\psi} = 0\cdot 119\, \bar{I}_{\xi\xi})$,
$I_{\phi\phi} = 22\cdot 4 \times 10^5\ (f_\phi = 1\cdot 46)$,
$\bar{I}_{\phi\phi} = 25\cdot 3 \times 10^5\ (\bar{f}_\phi = 1\cdot 38)$,
$I_{\xi\phi} = 836$.

Test Number	$1/n$	μ	Speed Range for Flutter		Critical Frequencies	
			V_c	$\bar{V}_c$	f_c	$\bar{f}_c$
1	0·052	28	120	195	1·45	1·52
2	0·061		121	195	1·46	1·53
3	0·073		117	191	1·46	1·52
4	0·077		123	193	1·46	1·52
5	0·095		138	201	1·46	1·52
6	0·107		139	185	1·45	1·52
7	0·107		134	208	1·45	1·50
8	0·112		No flutter		—	—
9	0·126		98	162	1·46	1·50
10	0·133		96	161	1 48	1·51
11	0·145		105	166	1·47	1·51
12	0·158		104	171	1·46	1·51
13	0·183		106	171	1·46	1·51
14	0·284		107	176	1·46	1·52
15	0·052	32	128	189	1·45	1·52
16	0·061		128	190	1·44	1·52
17	0·073		136	186	1·46	1·50
18	0·077		130	191	1·46	1·51
19	0·095		140	179	1·46	1·50
20	0·107		No flutter		—	—
21	0·112		No flutter		—	—
22	0·126		119	155	1·47	1·50
23	0·133		112	156	1·47	1·50
24	0·145		107	167	1·47	1·51
25	0·158		108	172	1·46	1·51
26	0·183		112	177	1·47	1·52
27	0·284		111	179	1·46	1·52
28	0·052	51	126	197	1·45	1·53

TABLE 3—*continued*

Test Number	$1/n$	μ	Speed Range for Flutter		Critical Frequencies	
			V_c	$\bar{V}_c$	f_c	$\bar{f}_c$
29	0·061	51	126	197	1·45	1·52
30	0·070		133	198	1·46	1·53
31	0·077		131	198	1·45	1·52
32	0·094		146	186	1·47	1·52
33	0·107		No flutter		—	—
34	0·112		No flutter		—	—
35	0·126		117	157	1·47	1·51
36	0·133		114	167	1·47	1·51
37	0·145		111	173	1·46	1·51
38	0·158		110	177	1·46	1·52
39	0·183		113	177	1·46	1·52
40	0·284		113	184	1·46	1·52
41	0·052	71	126	199	1·46	1·54
42	0·061		127	197	1·46	1·53
43	0·073		130	194	1·46	1·52
44	0·077		130	197	1·46	1·53
45	0·094		131	190	1·47	1·52
46	0·107		132	190	1·46	1·52
47	0·112		131	185	1·47	1·52
48	0·126		127	186	1·46	1·52
49	0·133		128	185	1·46	1·51
50	0·145		125	185	1·46	1·51
51	0·158		122	185	1·46	1·51
52	0·183		124	187	1·46	1·52
53	0·284		126	188	1·46	1·52
54	0·052	280	130	193	1·46	1·53
55	0·061		123	193	1·46	1·52
56	0·077		125	192	1·46	1·52
57	0·094		123	192	1·47	1·53
58	0·107		123	193	1·48	1·52
59	0·112		123	195	1·45	1·52
60	0·126		122	192	1·45	1·52
61	0·133		125	192	1·46	1·53
62	0·145		124	194	1·45	1·53
63	0·158		125	193	1·45	1·53
64	0·183		124	197	1·46	1·53
65	0·284		125	197	1·46	1·54

TABLE 4

Results for Antisymmetrical Flutter with a Balanced Aileron-carried Damper—Altitude 30,000 ft

General Conditions

(a) *Stiffnesses* $l_\xi = 0$,

$l_\phi = 1\cdot892 \times 10^8$.

(b) *Inertias* $I_{\psi\psi} = 5\cdot73$, $I_{\psi\phi} = 0$,

$I_{\xi\xi} = 44\cdot8$ $(I_{\psi\psi} = 0\cdot128 I_{\xi\xi})$,

$I_{\phi\phi} = 22\cdot5 \times 10^5$ $(f_\phi = 1\cdot46)$,

$I_{\xi\phi} = 836$.

Test Number	μ	Lower Critical Speed			Upper Critical Speed		
		V_c	f_c	$1/n$	$\bar{V}_c$	$\bar{f}_c$	$1/\bar{n}$
66	11	166	1·46	0·0724	347	1·75	0·068
67		165	1·46	0·081	350	1·76	0·075
68		168	1·49	0·087	348	1·76	0·081
69		165	1·47	0·093	356	1·76	0·085
70		173	1·44	0·104	380 app.	—	—
71		177	1·43	0·110	346	1·59	0·102
72		185*	1·47	0·110	334	1·74	0·098
73		153	1·46	0·115	331	1·73	0·099
74		155	1·45	0·119	333	1·73	0·104
75		157	1·49	0·120	336	1·74	0·105
76		157	1·47	0·124	333	1·76	0·107
77		159	1·47	0·1313	336	1·76	0·111
78	19	172	1·47	0·072	349	1·74	0·069
79		170	1·44	0·082	351	1·74	0·076
80		170	1·44	0·088	350	1·74	0·081
81		171	1·47	0·093	357	1·74	0·085
82		175	1·45	0·103	342	1·70	0·086
83		175	1·47	0·108	336	1·77	0·079
84		157	1·48	0·109	333	1·72	0·099
85		152	1·47	0·114	333	1·73	0·101
86		153	1·46	0·116	334	1·73	0·103
87		154	1·47	0·118	335	1·74	0·103
88		156	1·46	0·122	336	1·74	0·106
89		156	1·46	0·125	337	1·74	0·107
90		160	1·45	0·133	339	1·74	0·112
91	25	170	1·44	0·073	352	1·74	0·069
92		169	1·45	0·088	350	1·75	0·081
93		169	1·45	0·103	346	1·73	0·093
94		166	1·45	0·111	343	1·73	0·098
95		164	1·47	0·114	342	1·73	0·100
96		164	1·46	0·119	342	1·73	0·104
97		164	1·46	0·125	343	1·72	0·109
98		164	1·48	0·131	341	1·75	0·112

* Intermittent flutter between 125 and 185 ft/sec.

TABLE 5

Results for Antisymmetrical Flutter with an Unbalanced Aileron-carried Damper—Zero Altitude

General Conditions

(a) *Stiffnesses* $l_\xi = 0,$

$l_\phi = 1\cdot892 \times 10^8.$

(b) *Inertias* $I_{\xi\xi} = 46\cdot1,$

$\bar{I}_{\xi\xi} = 50\cdot9,$

$I_{\phi\phi} = 23\cdot2 \times 10^5 \quad (f_\phi = 1\cdot46,)$

$\bar{I}_{\phi\phi} = 26\cdot2 \times 10^5 \quad (\bar{f}_\phi = 1\cdot35),$

$I_{\xi\phi} = 836,$

$I_{\psi\phi} = -297.$

Test Number	$1/n$	μ	Speed Range for Flutter V_c	$\bar{V}_c$	Critical Frequencies f_c	$\bar{f}_c$
$I_{\psi\psi} = 12\cdot64$						
99	0·091	28	No flutter		—	—
100	0·159		No flutter		—	—
101	0·167		126	190	1·47	1·57
102	0·198		90	187	1·48	1·55
103	0·272		103	183	1·47	1·55
104	0·421		106	182	1·47	—
$I_{\psi\psi} = 13\cdot25$						
105	0·079	32	No flutter		—	—
106	0·105		No flutter		—	—
107	0·162		82	186	1·48	1·57
108	0·172		91	189	1·47	1·56
109	0·203		97	187	1·47	1·55
110	0·431		111	183	1·47	1·58
111	0·058	71	No flutter		—	—
112	0·162		No flutter		—	—
113	0·172		117	167	1·48	1·52
114	0·203		119	172	1·49	1·54
115	0·431		118	181	1·46	1·52
116	0·058	280	No flutter		—	—
117	0·203		No flutter		—	—
118	0·278		136	176	1·47	1·56
119	0·431		131	180	1·47	1·57
120	Damper disc locked to aileron.		148	164	1·48	1·49

REFERENCES

No.	*Author*	*Title, etc.*
1	C. Scruton	Wing Flexure-aileron Flutter Tests on a Model of B.A.C. Wing Type 167. R. & M. 2480. October, 1944.
2	W. P. Jones	Effect of a Flexurally-geared Aileron Control on Binary flutter of a Wing-aileron System. R. & M. 2362. February, 1944.
3	C. Scruton	Experimental Determination of the Aerodynamic Derivatives for Flexural-aileron Flutter of B.A.C. Wing Type 167. R. & M. 2373. May, 1945.

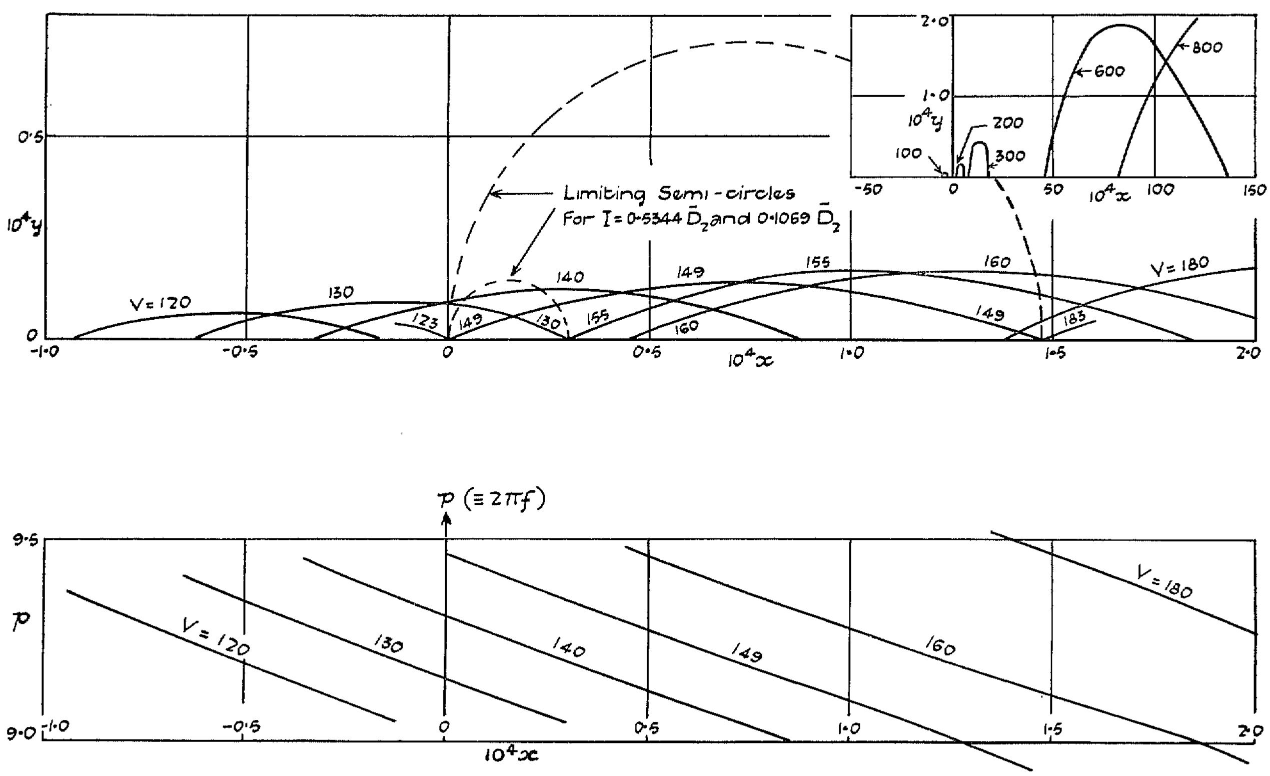

FIG. 3. (x, y) diagram for balanced aileron-carried damper. Tank empty ; $h = 0$, $h_\xi = 0$.

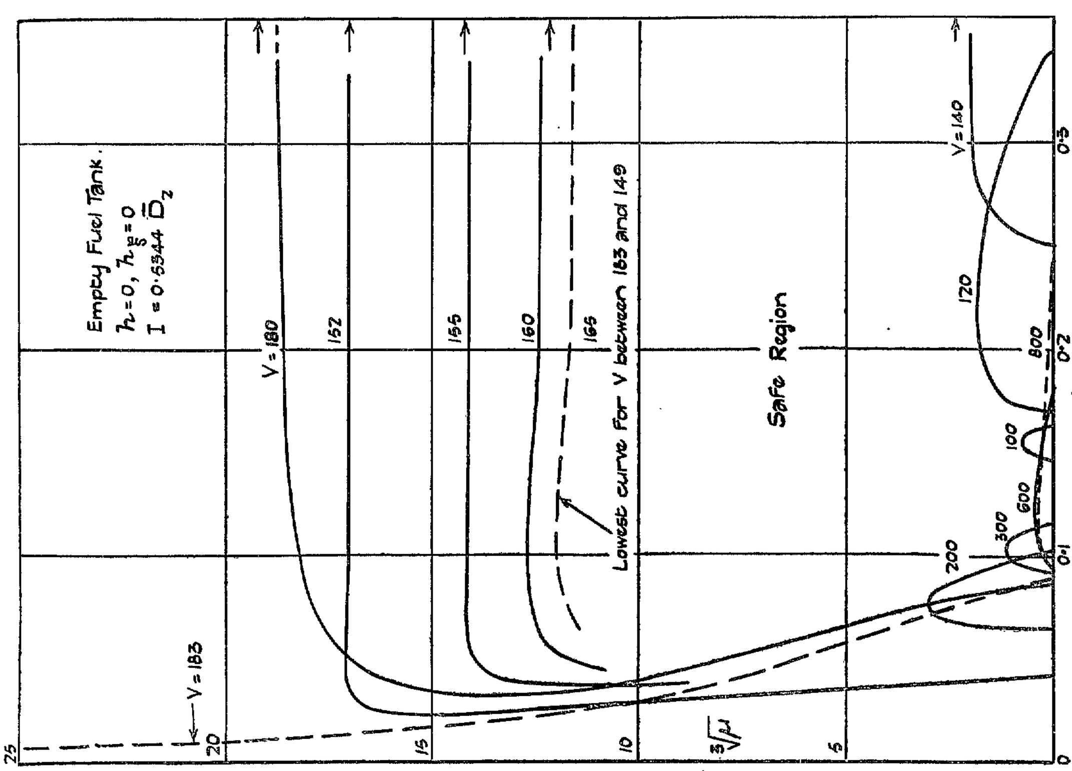

FIG. 4. Intermediate diagram for balanced aileron-carried damper.

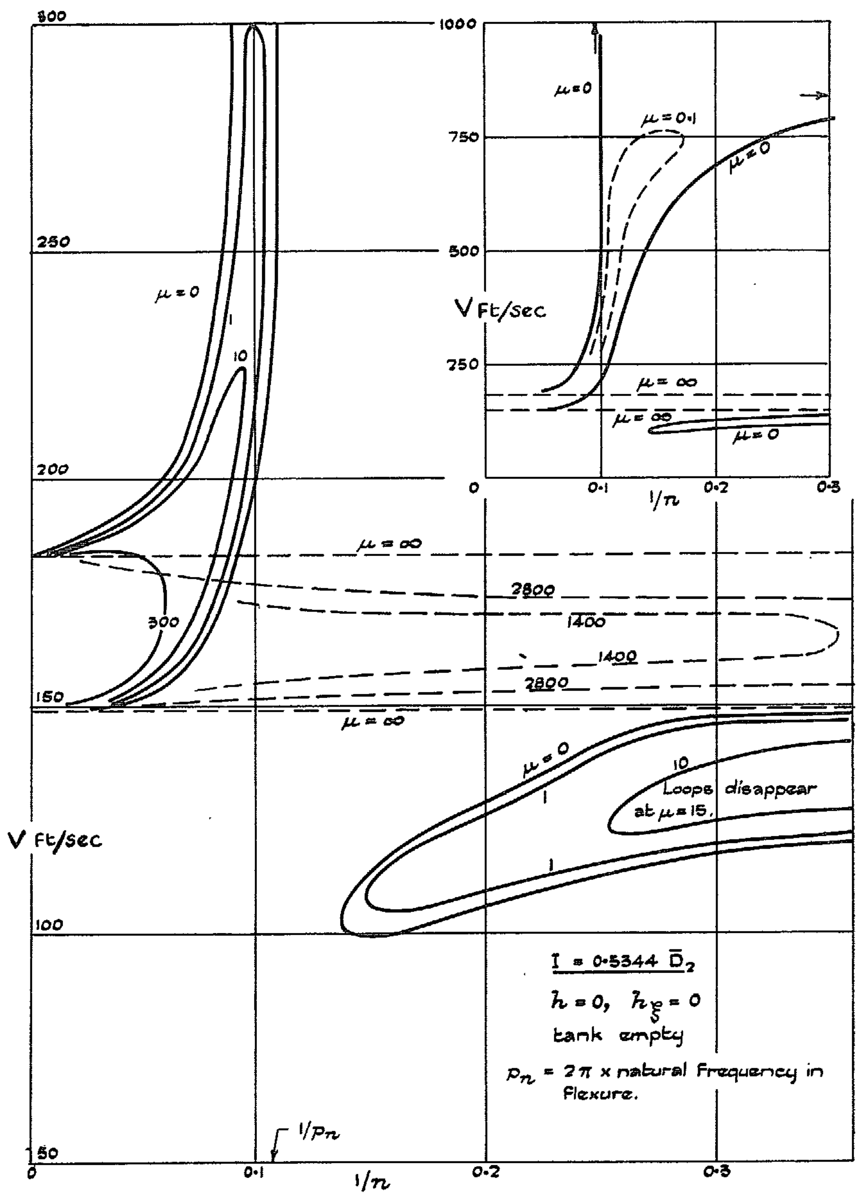

FIG. 5. Final damping diagram for balanced aileron-carried damper.

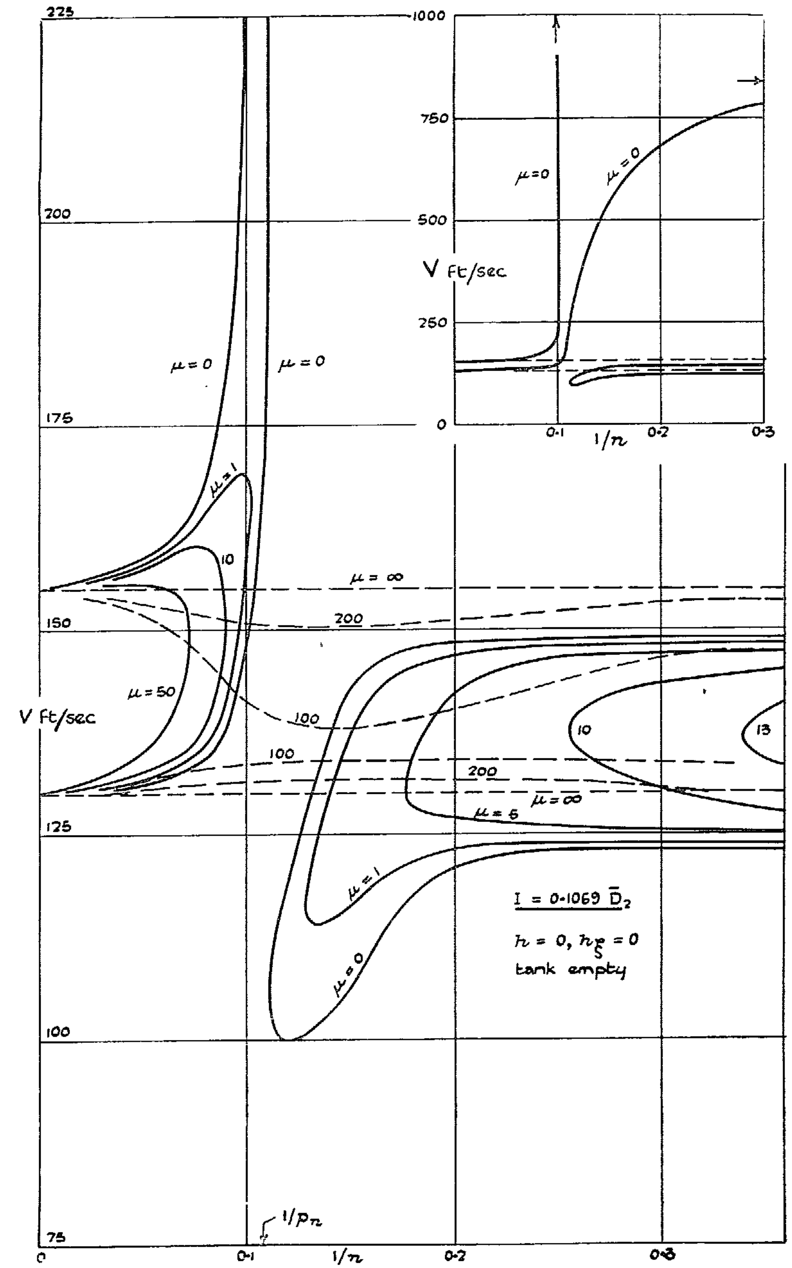

FIG. 6. Final damping diagram for balanced aileron-carried damper.

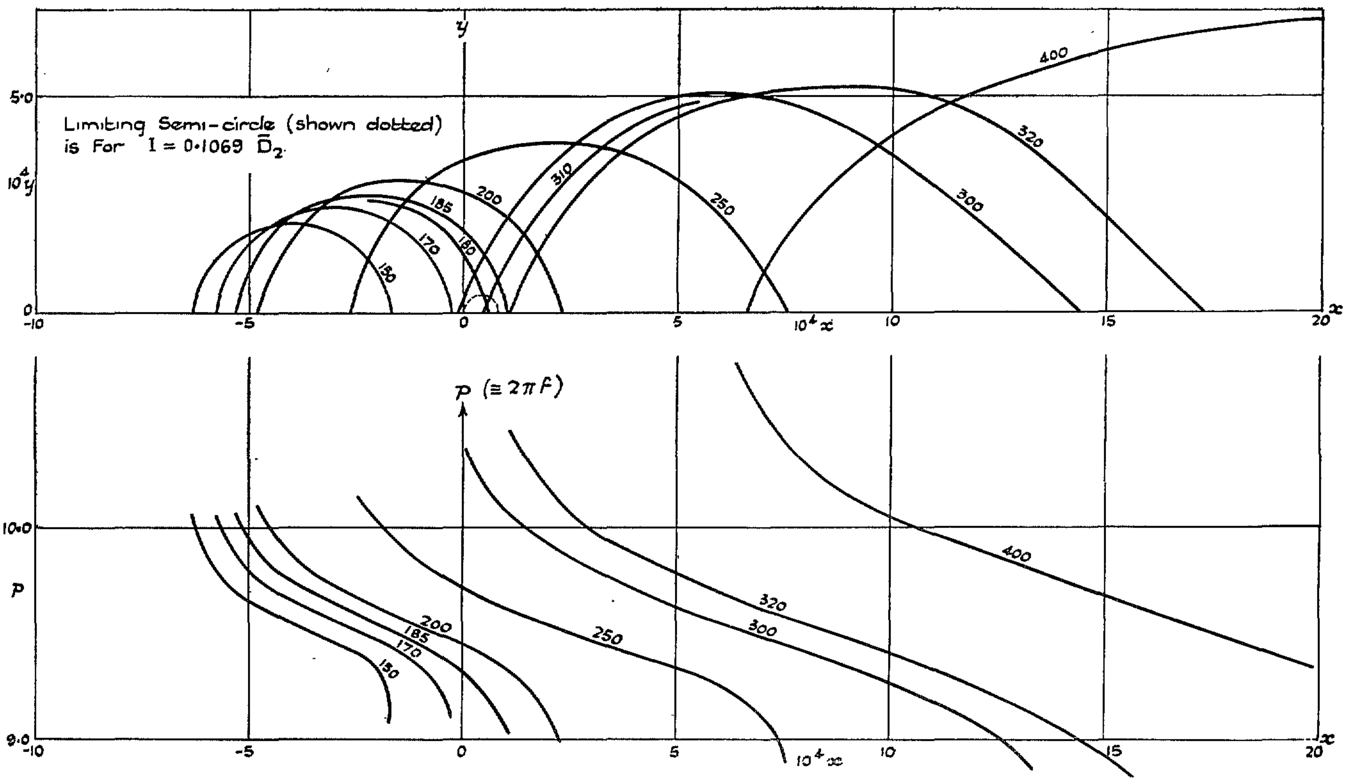

FIG. 7. (x, y) diagram for balanced aileron-carried damper. Tank empty; $h = 30{,}000$, $h_\xi = 0$.

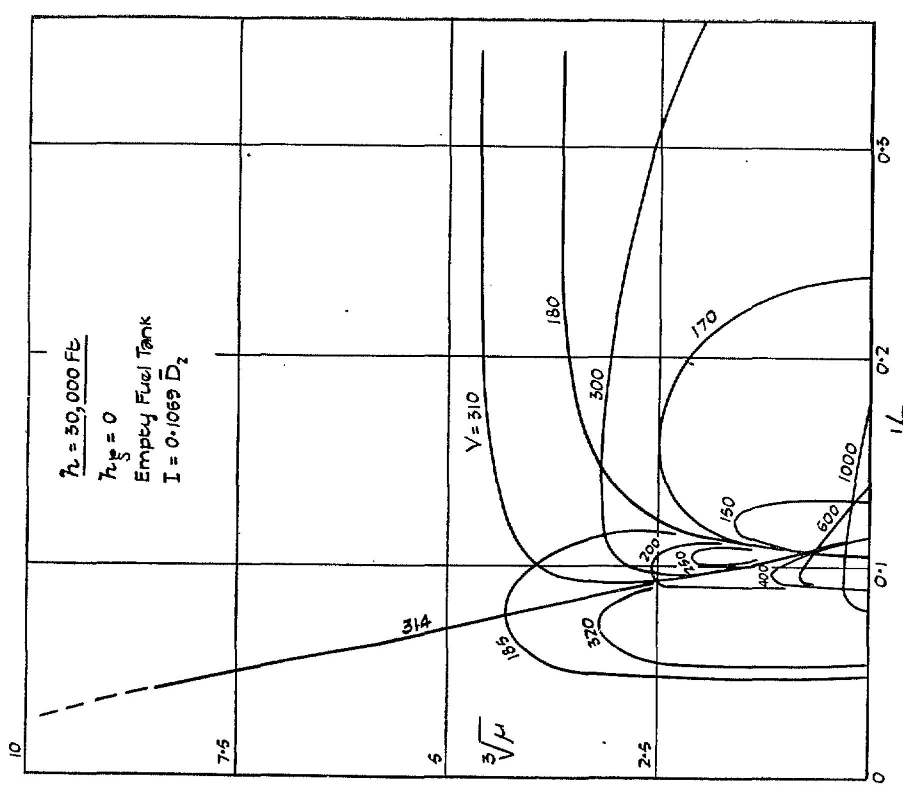

FIG. 8. Intermediate diagram for balanced aileron-carried damper.

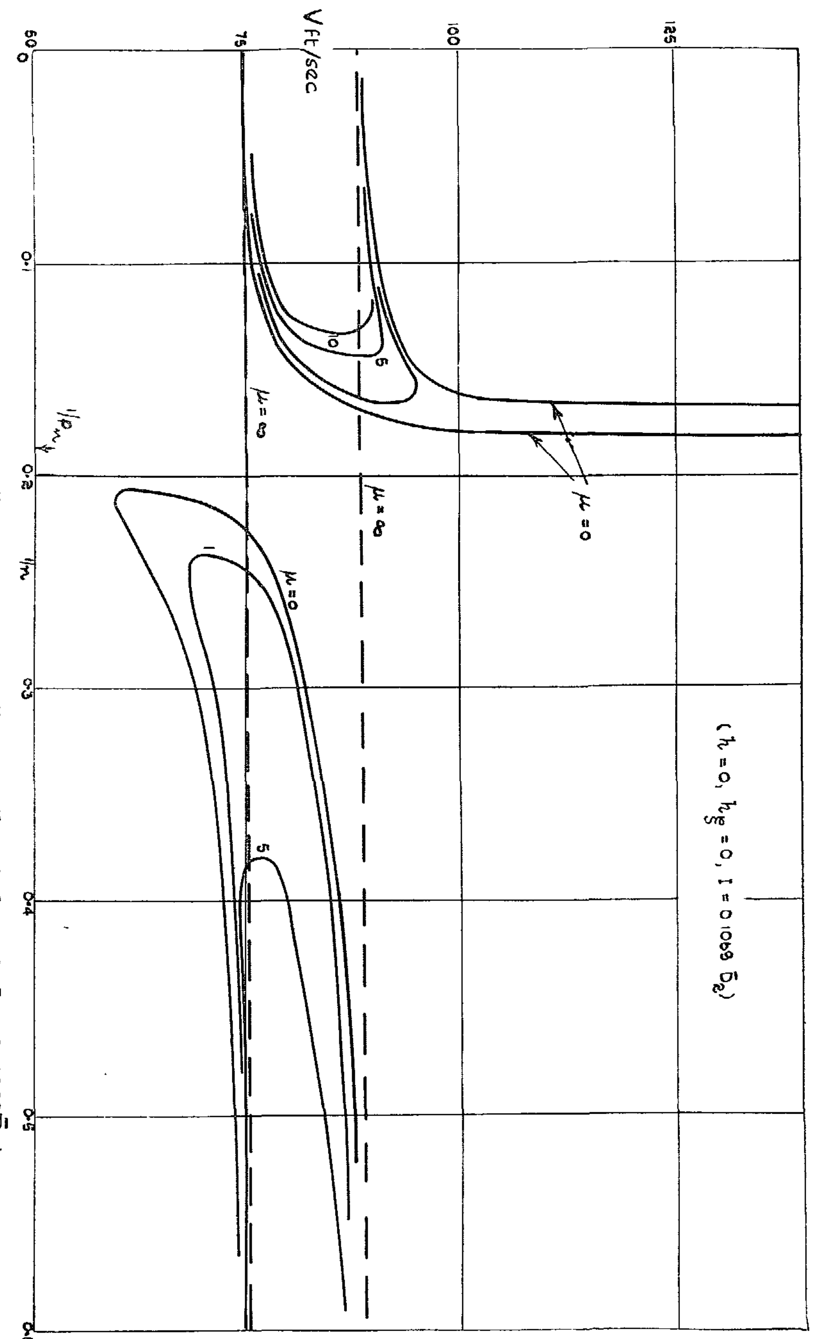

FIG. 10. Final damping diagram for tank-full case. ($h = 0$, $h_\xi = 0$, $I = 0\cdot1069\bar{D}_2$.)

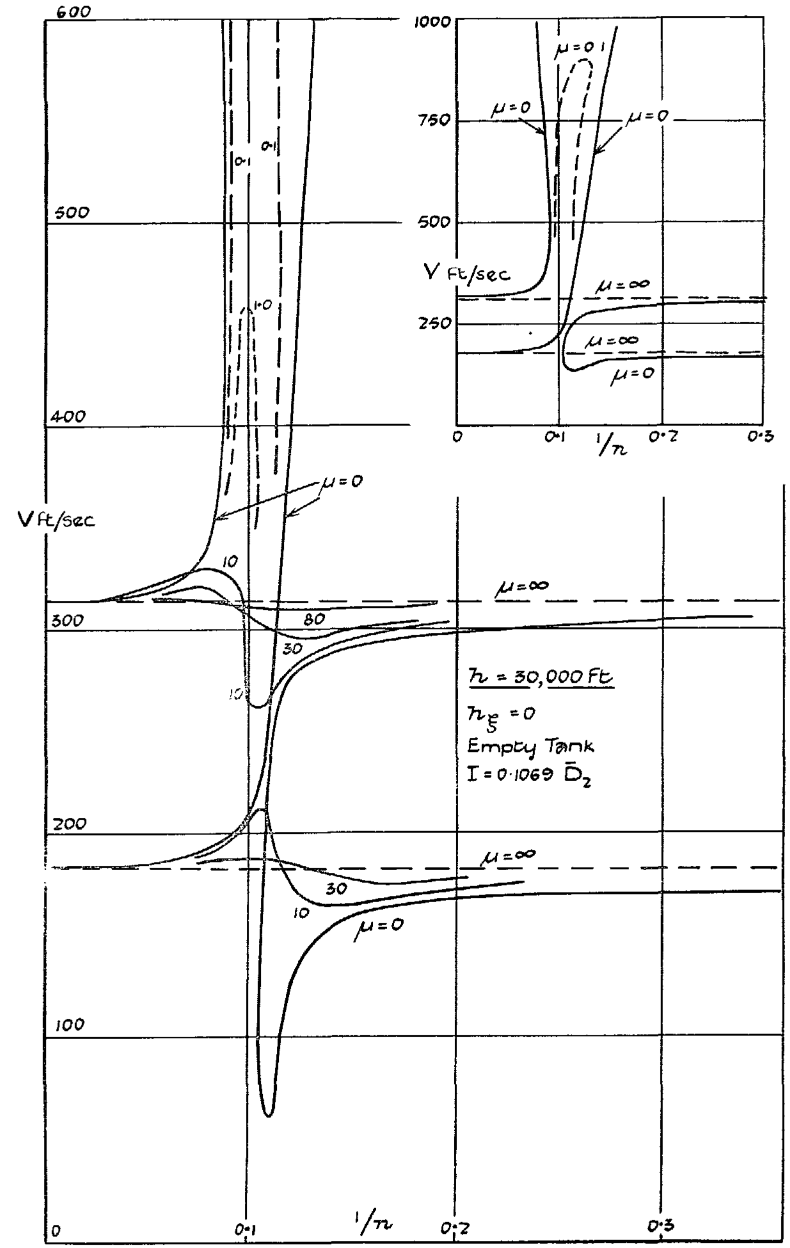

FIG. 9. Final damping diagram for balanced aileron-carried damper.

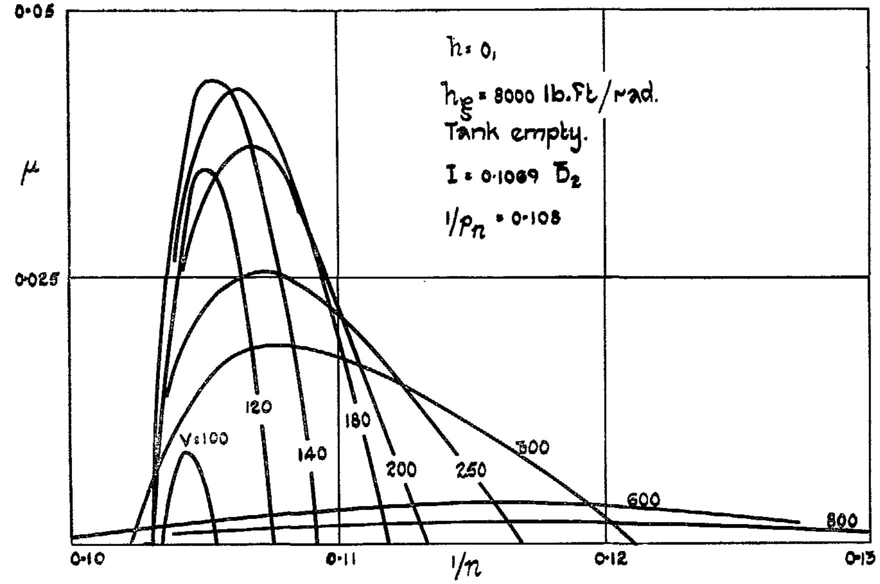

FIG. 12. Intermediate diagram for symmetrical flutter with balanced aileron-carried damper.

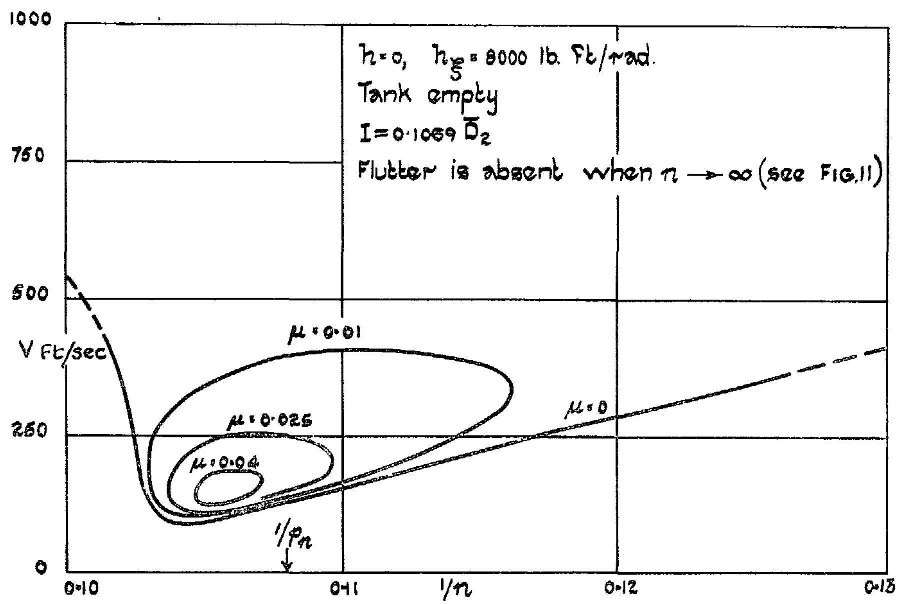

FIG. 13. Final damping diagram for symmetrical flutter with balanced aileron-carried damper.

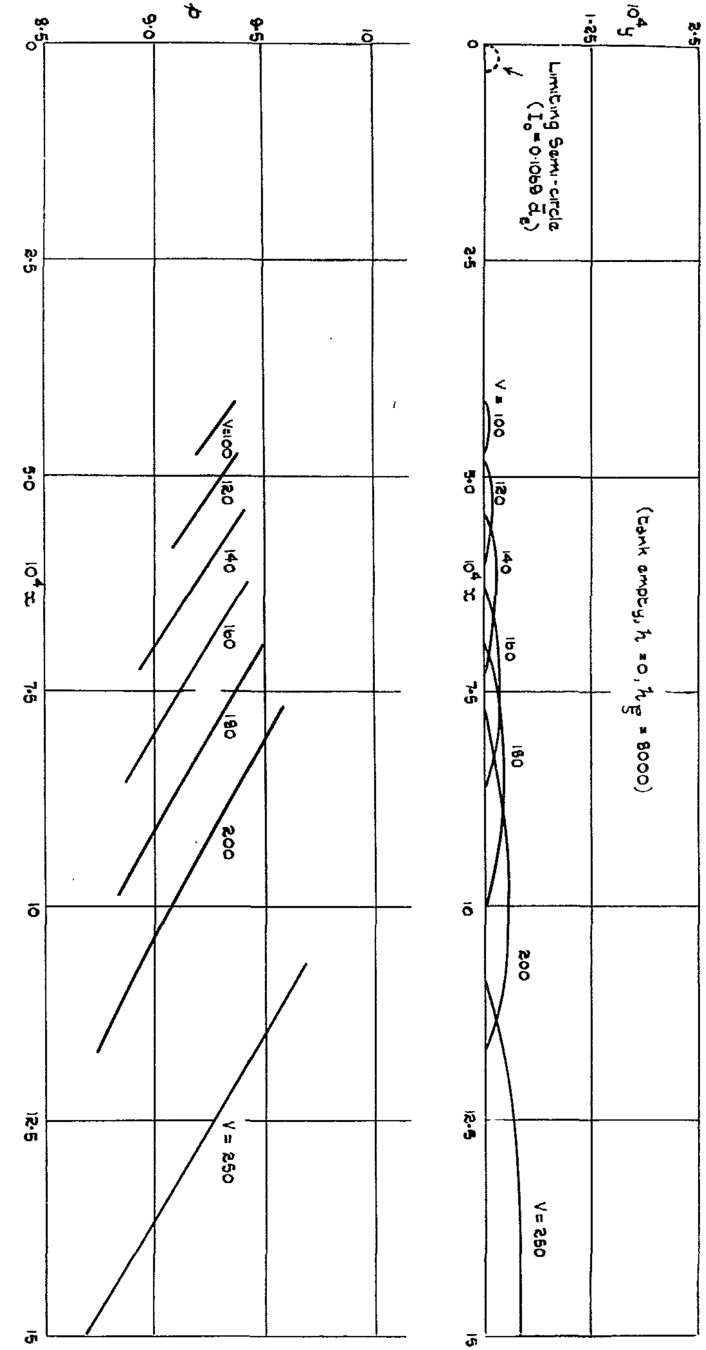

FIG. 11. (x, y) diagram for symmetrical flutter. Tank empty; $h = 0$, $h_\xi = 8{,}000$.

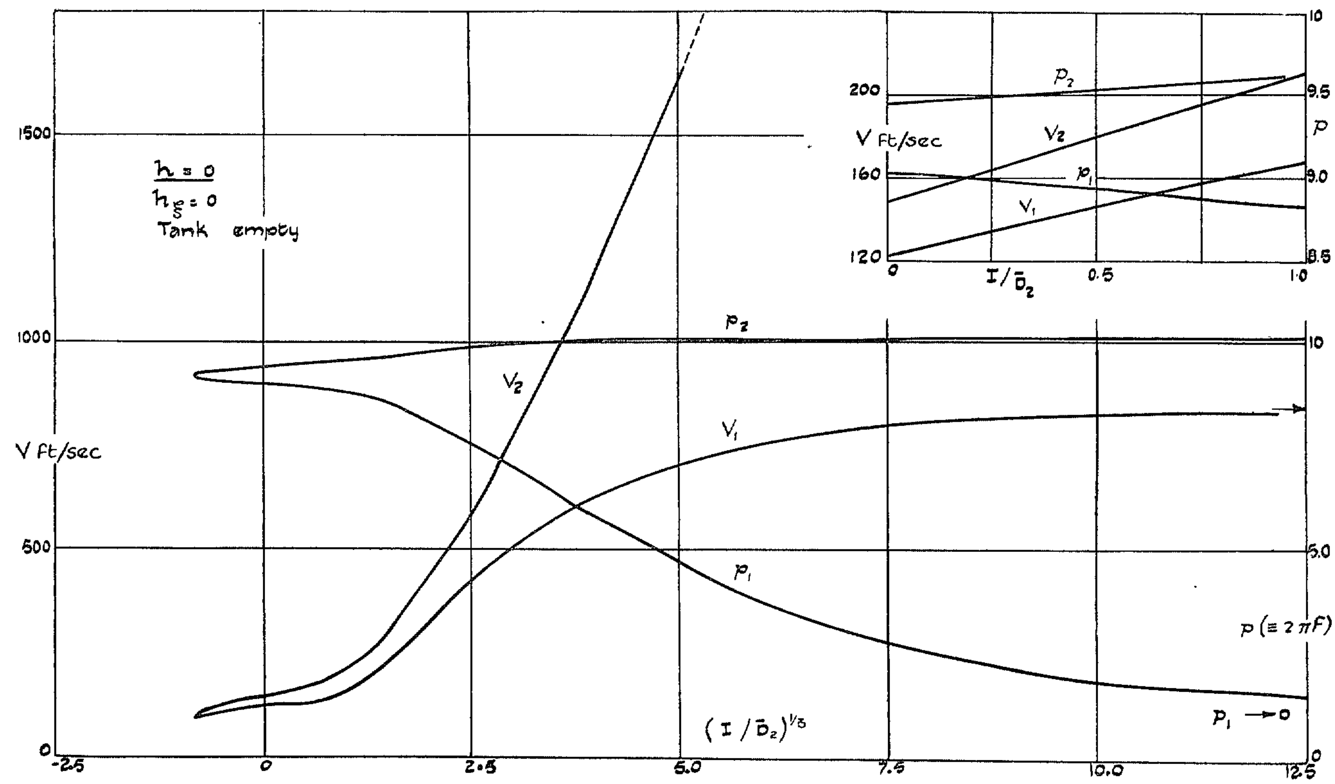

FIG. 14. Critical speeds and frequencies with casing locked to aileron.

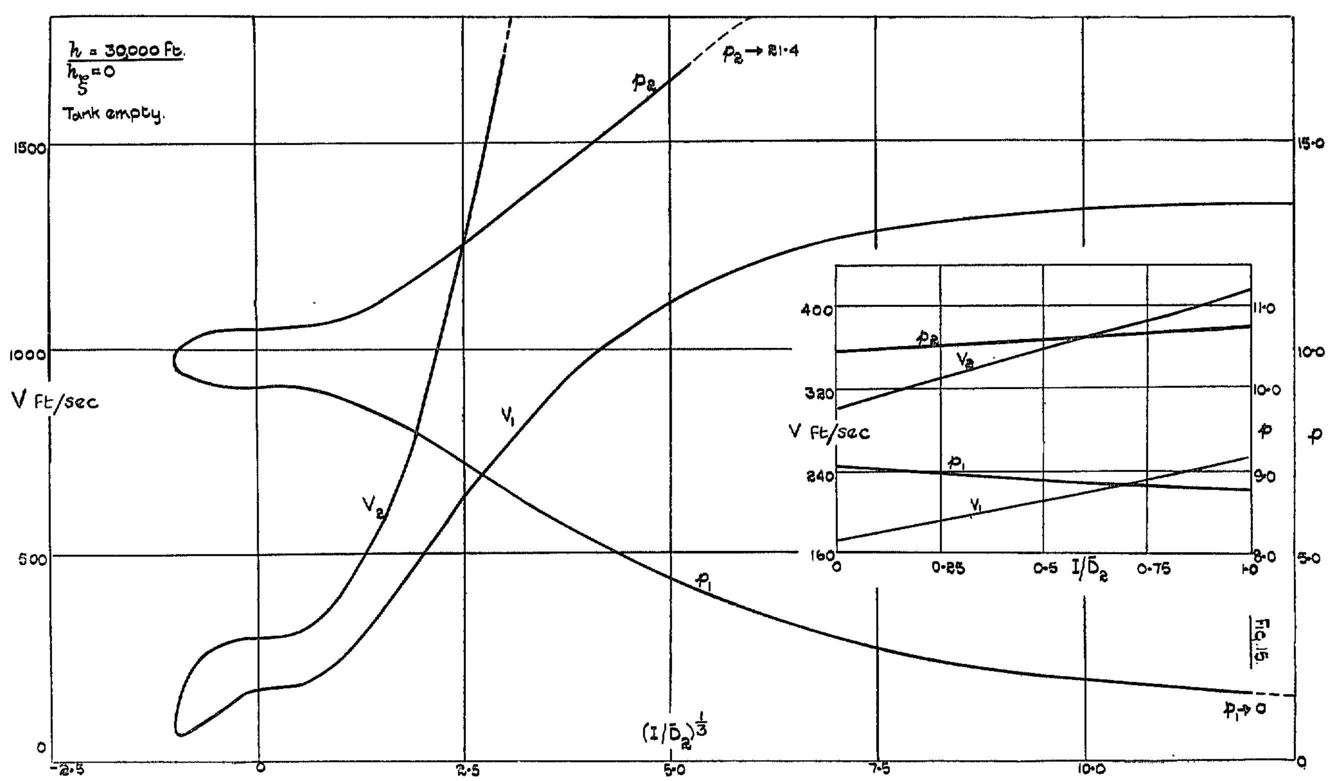

FIG. 15. Critical speeds and frequencies with casing locked to aileron.

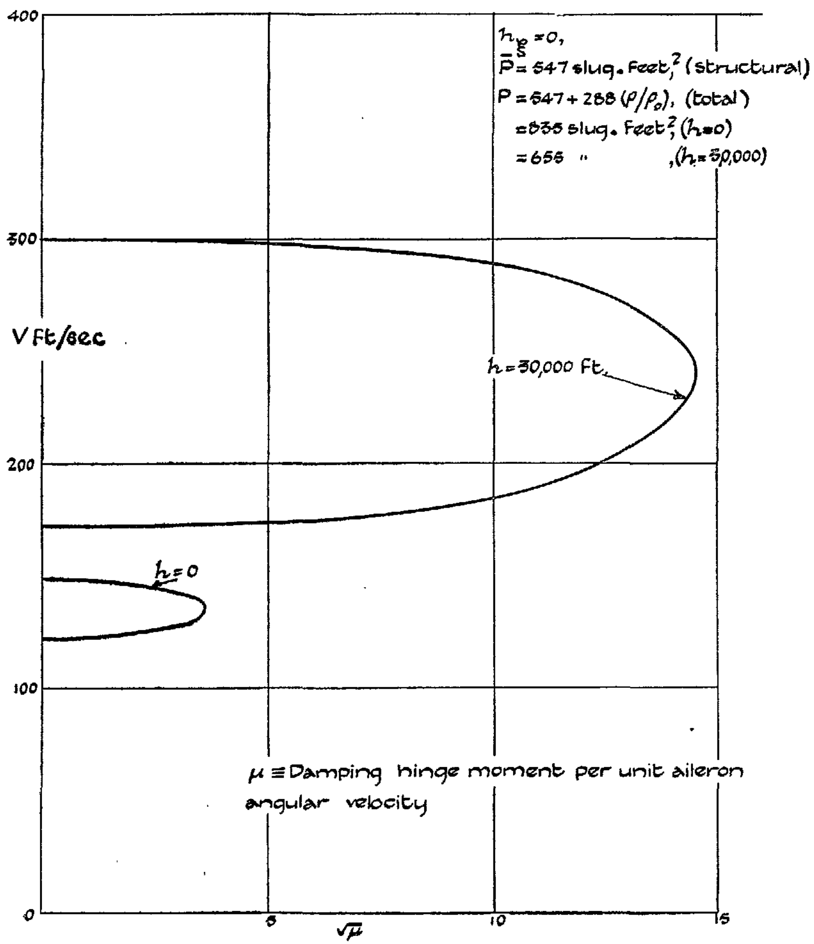

FIG. 16. Influence of plain artificial damping with casing locked to the wing.

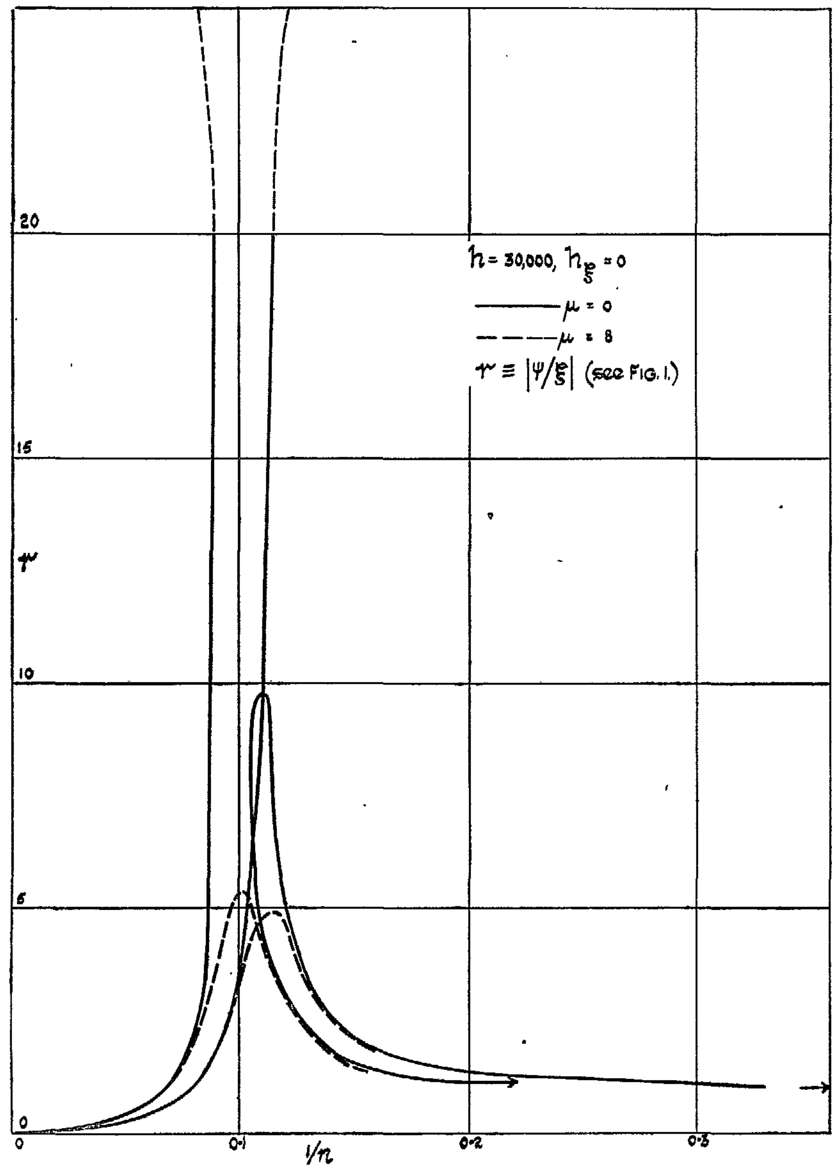

FIG. 17. Amplitude ratio diagram for case of Fig. 9.

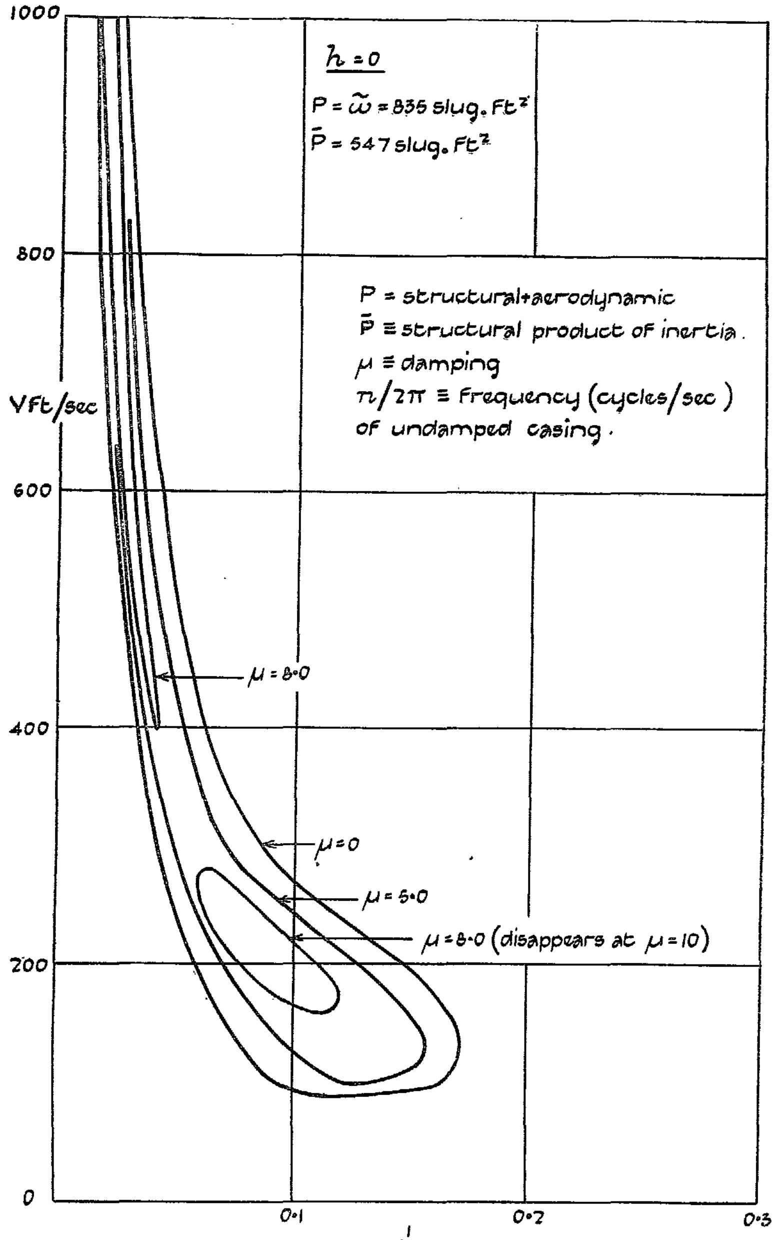

FIG. 18. Final damping diagram for a mass-balanced aileron-damper system.

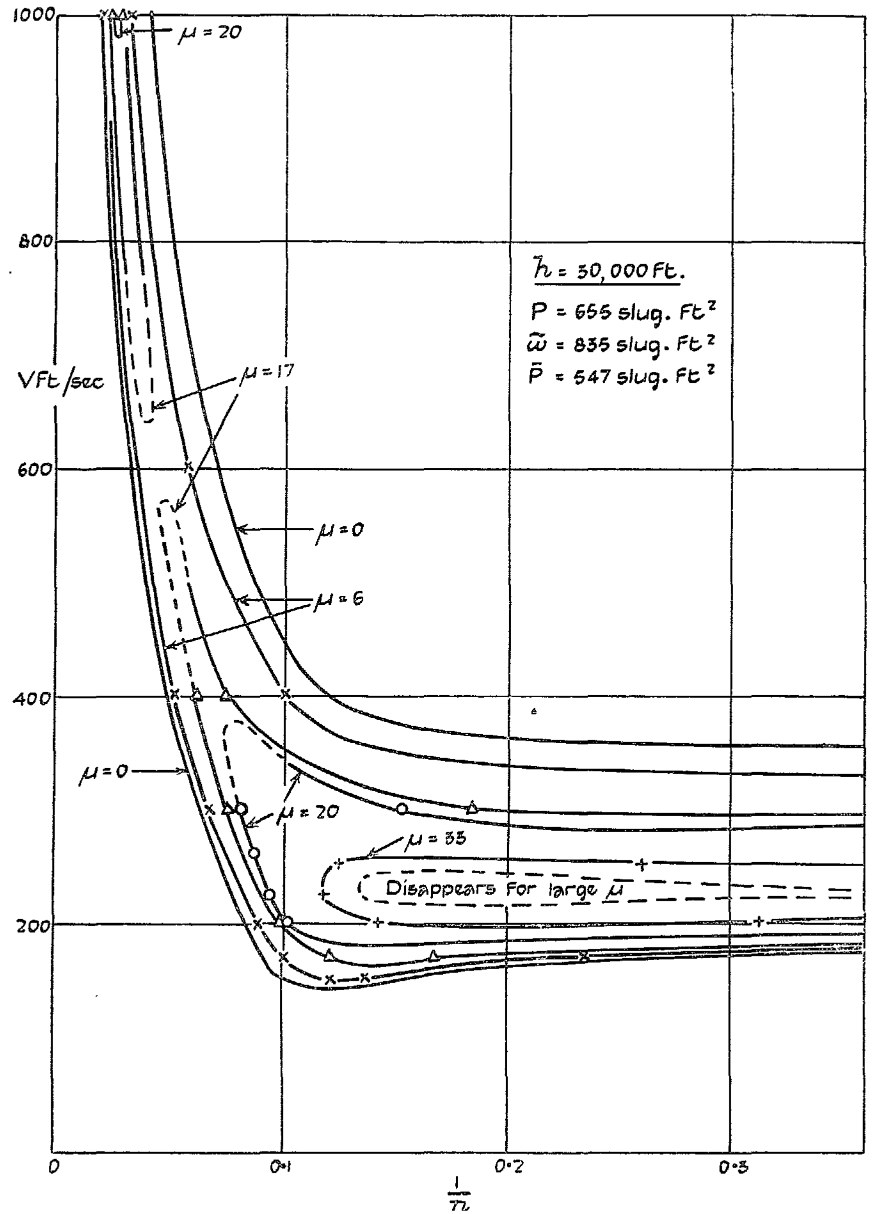

FIG. 19. Final damping diagram for an aileron-damper system mass-balanced at sea level (altitude effect).

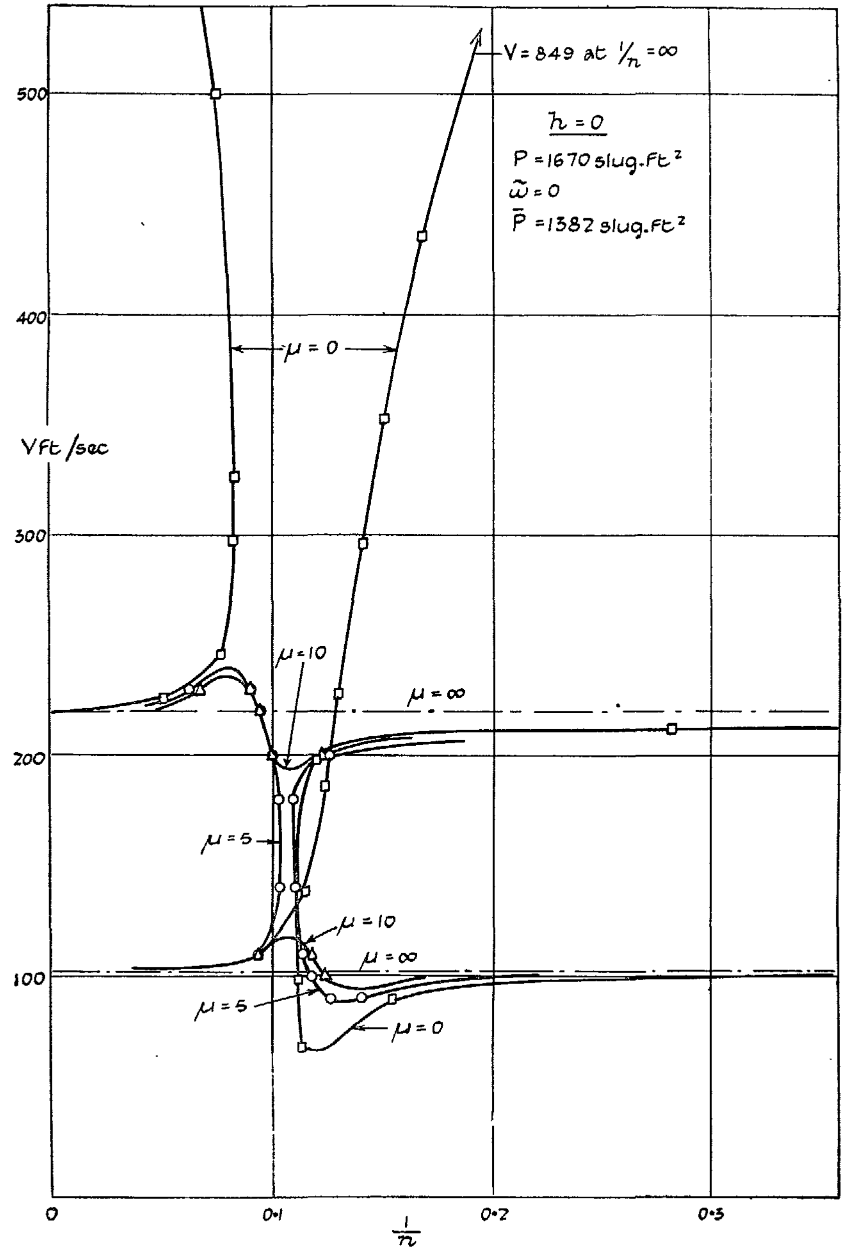

FIG. 20. Final damping diagram for a balanced aileron-carried damper.

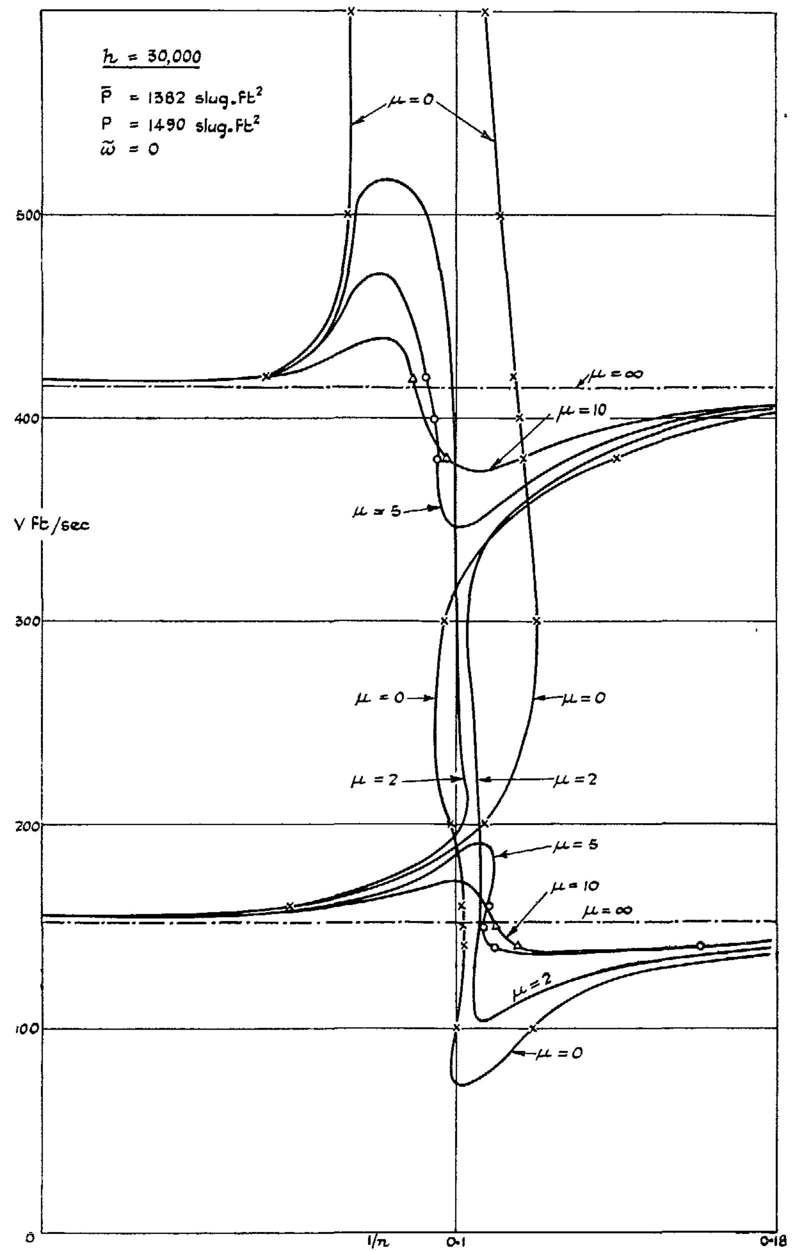

FIG. 21. Final damping diagram for a balanced aileron-carried damper (altitude effect).

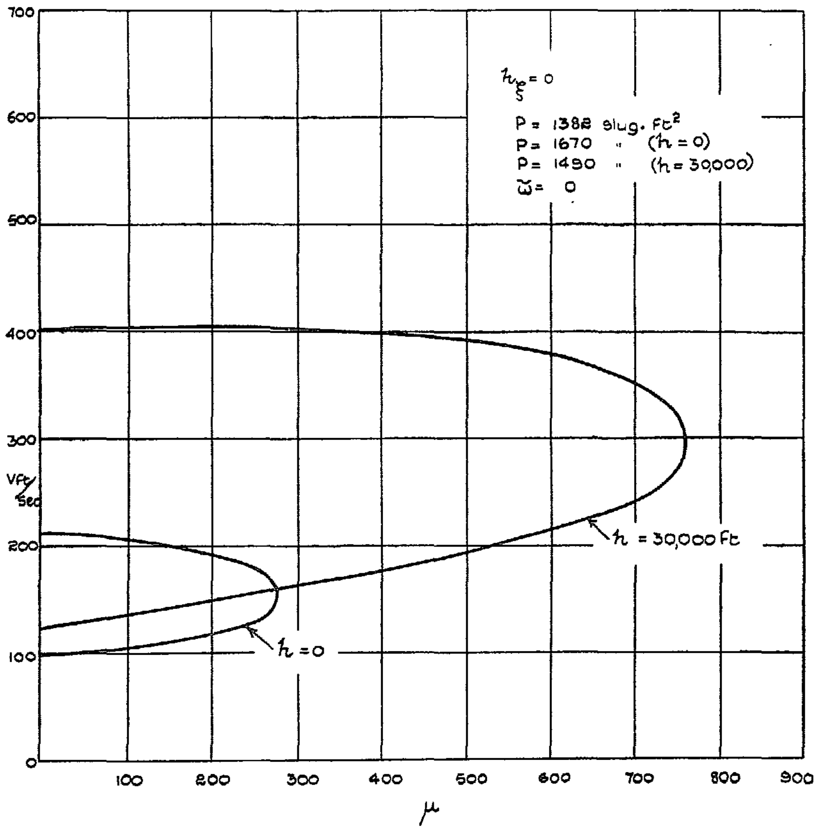

FIG. 22. Influence of plain artificial damping with casing locked to the wing.

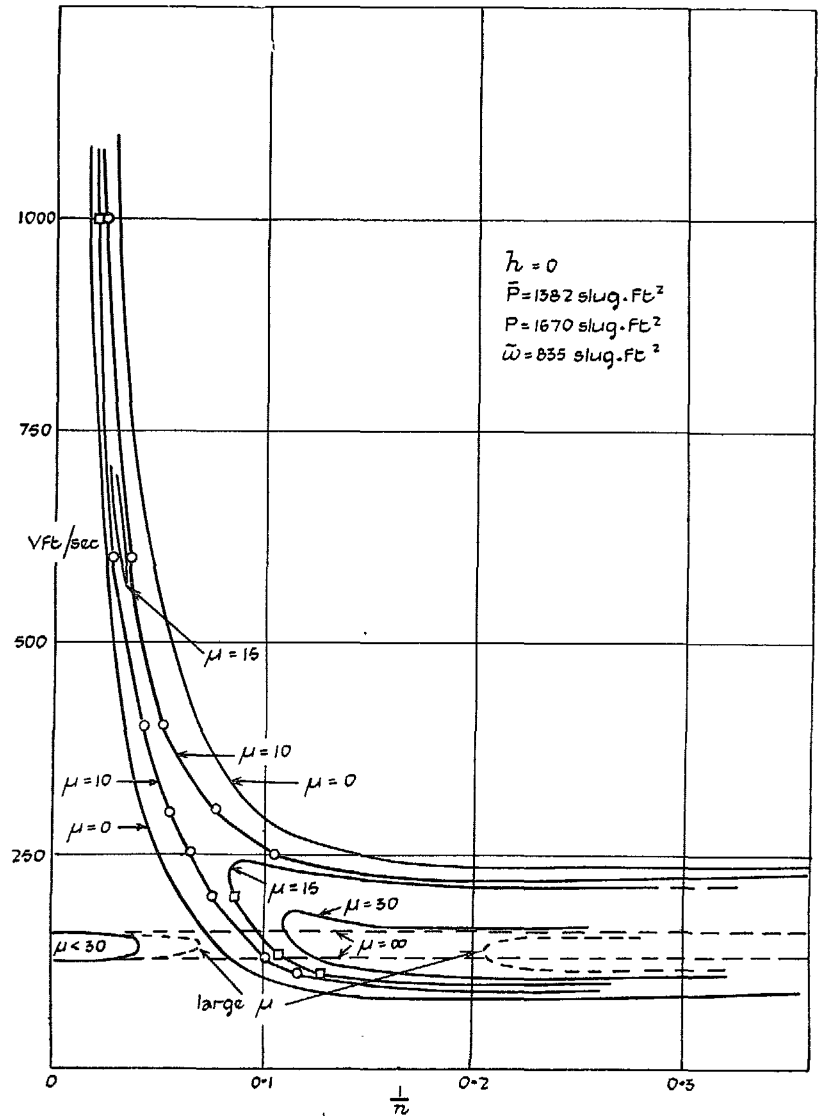

FIG. 23. Final damping diagram for a partly mass-balanced aileron-damper system.

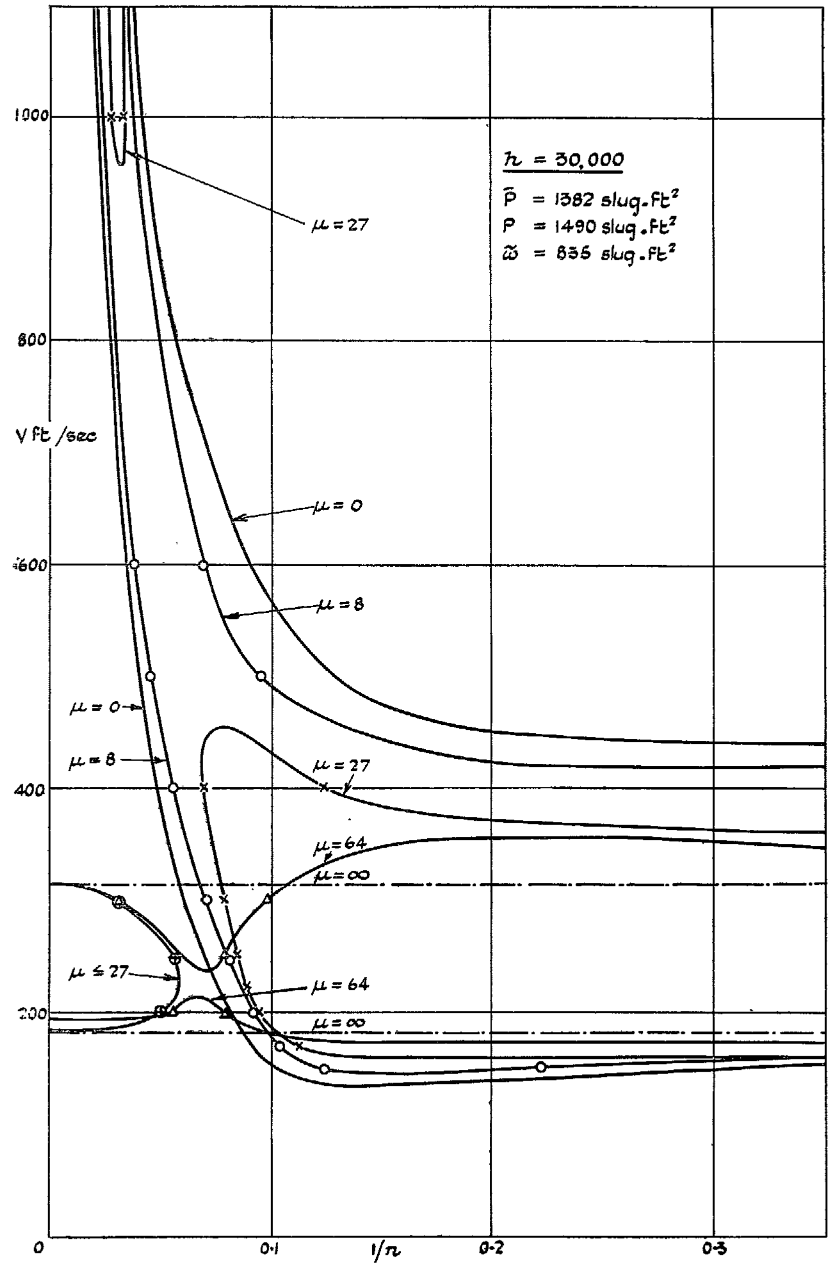

FIG. 24. Final damping diagram for a partly mass-balanced aileron-damper system (altitude effect).

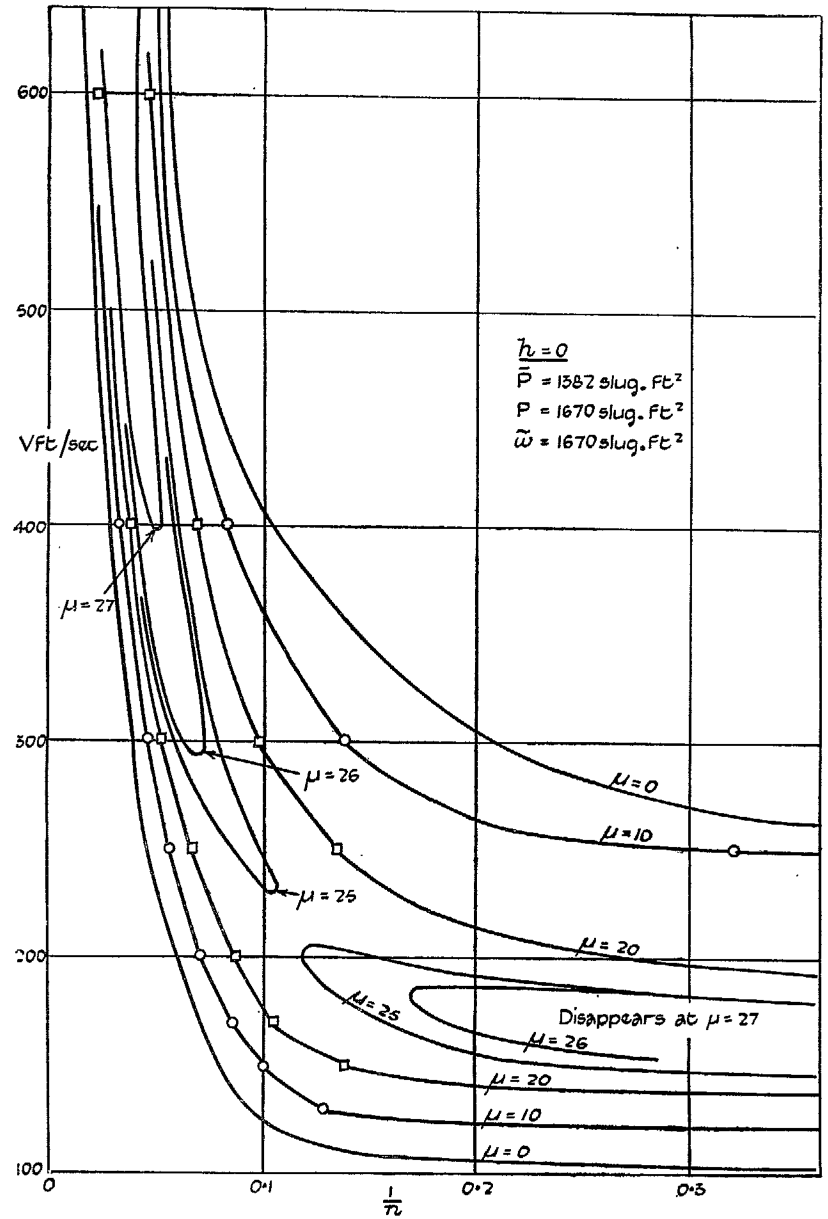

FIG. 25. Final damping diagram for a mass-balanced aileron-damper system.

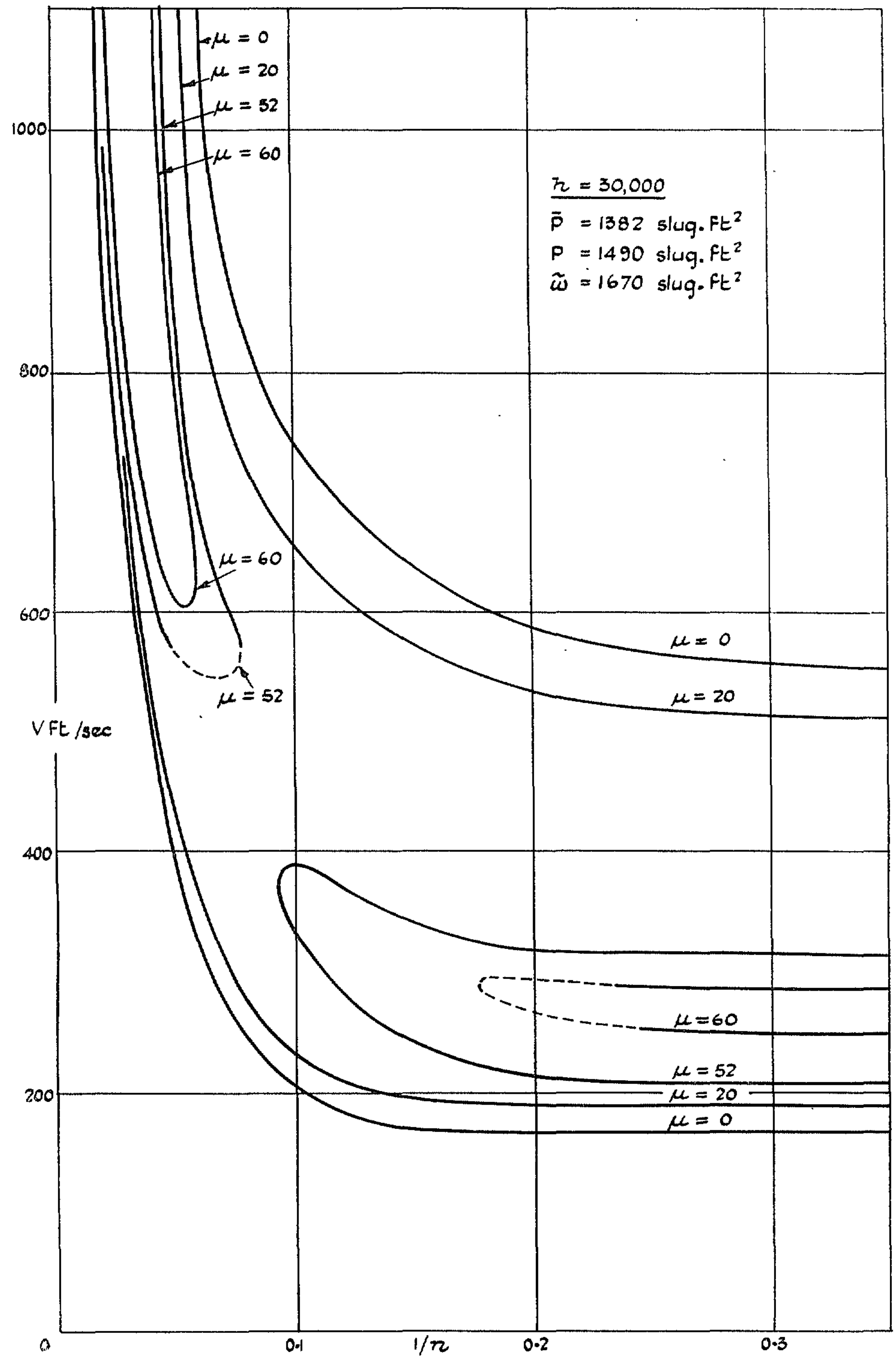

FIG. 26. Final damping diagram for a mass-balanced aileron-damper system (altitude effect).

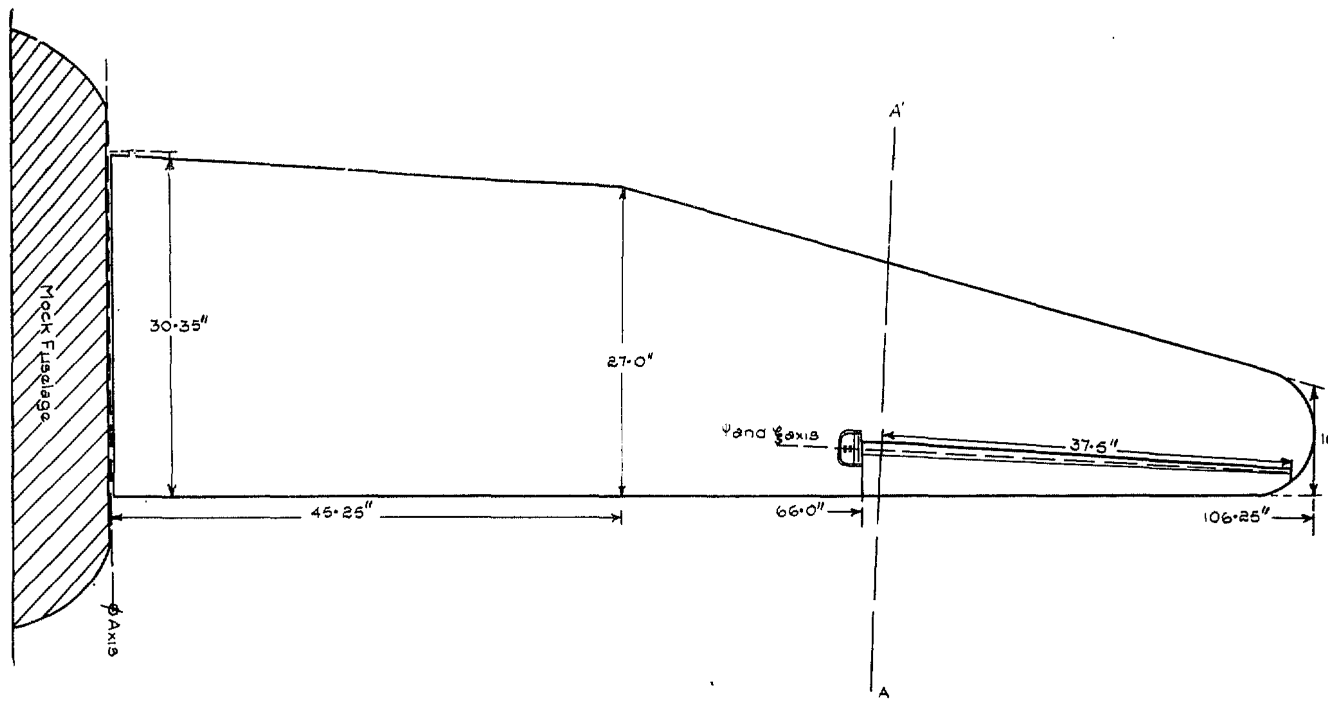

Fig. 27. Plan of wing.

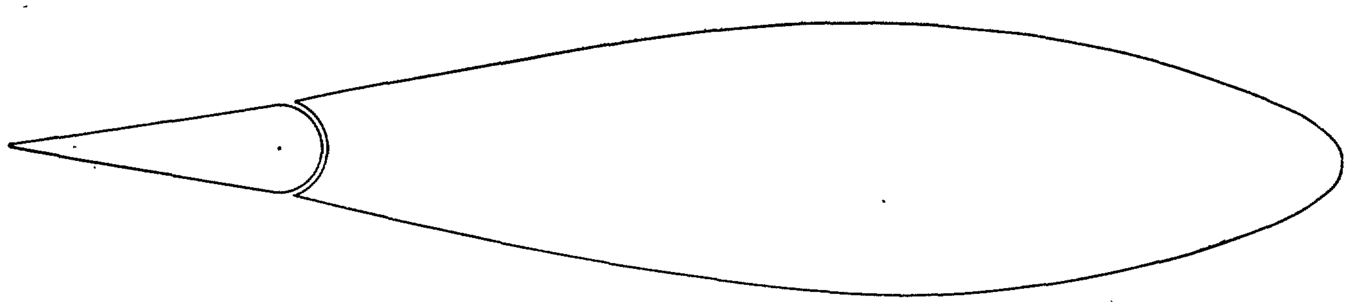

Fig. 28. Profile at section A–A′ of Fig. 27.

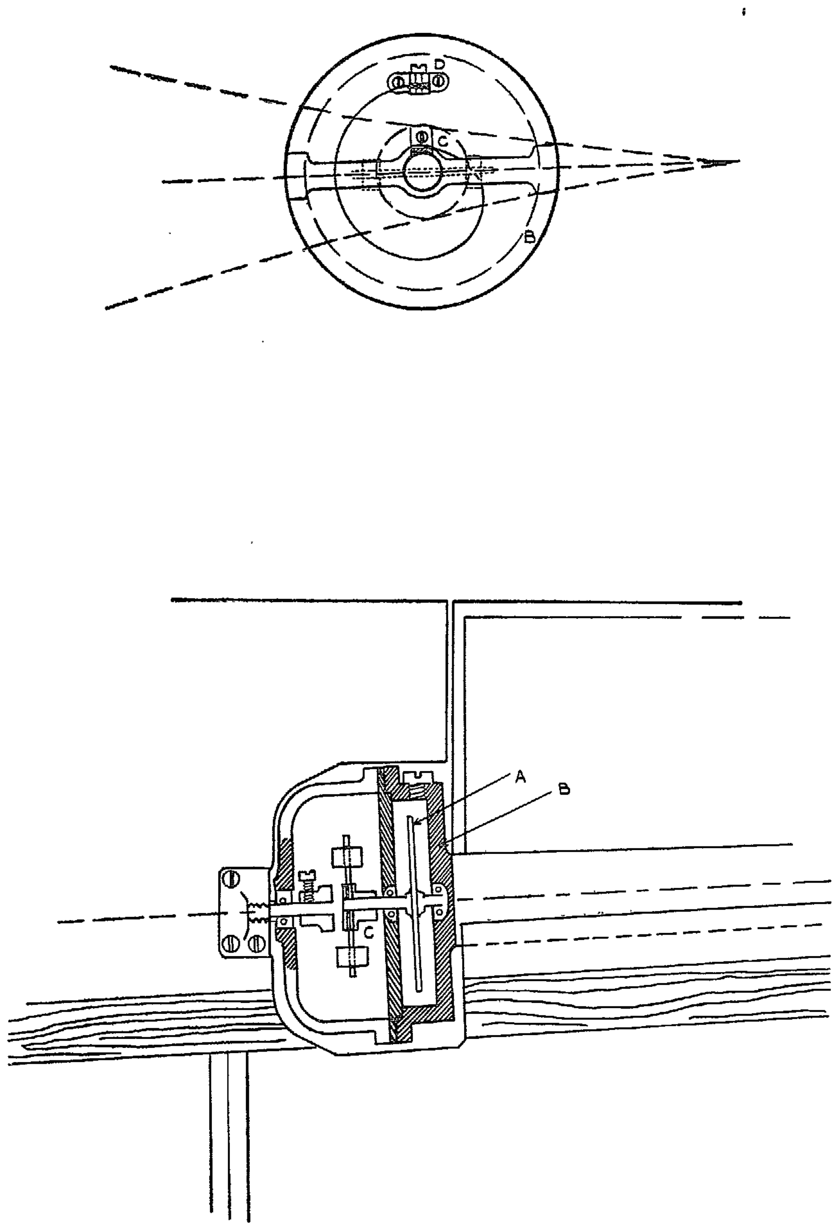

FIG. 29. Arrangement of damper.

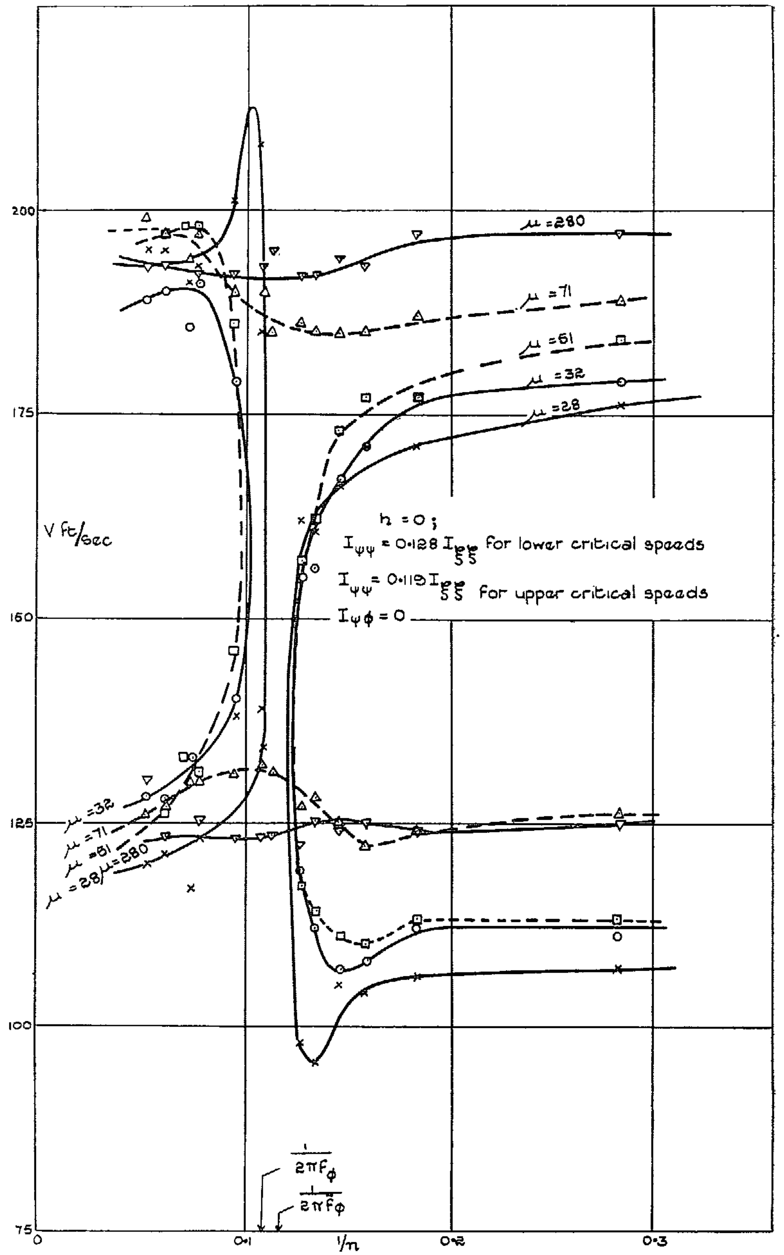

FIG. 30. Influence of balanced aileron-carried damper on antisymmetrical wing flexure-aileron flutter.

(93011) Wt. 18/806 K.5 12/52 Hw.

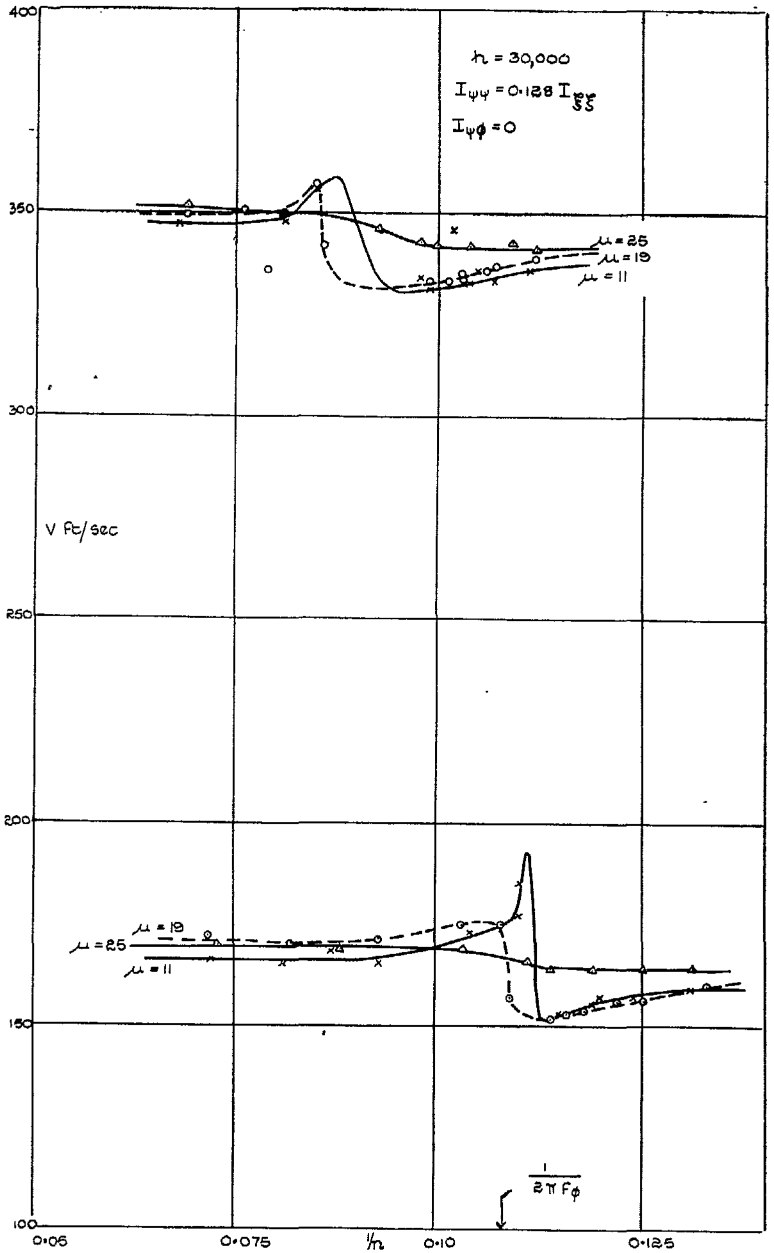

FIG. 31. Influence of balanced aileron-carried damper on antisymmetrical wing flexure-aileron flutter.

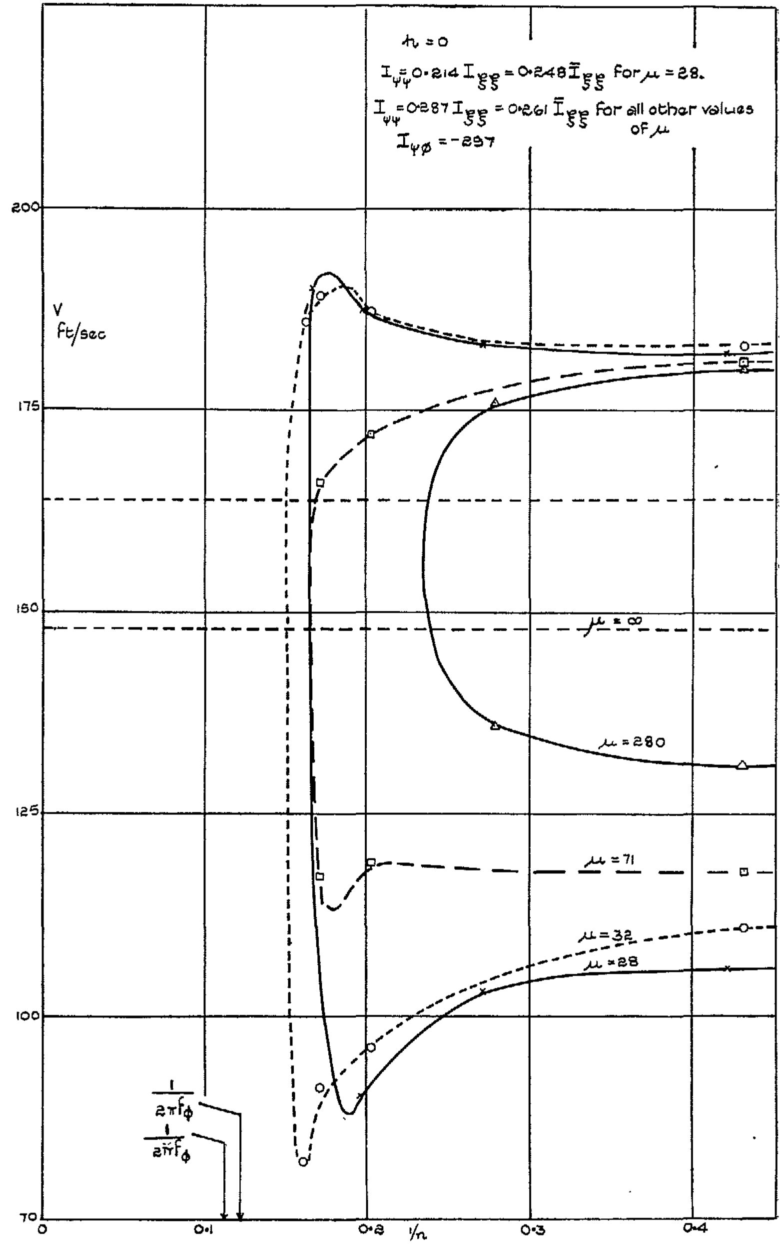

FIG. 32. Influence of unbalanced aileron-carried damper on antisymmetrical wing flexure-aileron flutter.

PRINTED IN GREAT BRITAIN

R. & M. No. 2559
(8581, 9946, 9882)
A.R.C. Technical Report

Publications of the Aeronautical Research Council

ANNUAL TECHNICAL REPORTS OF THE AERONAUTICAL RESEARCH COUNCIL (BOUND VOLUMES)—

1934–35 Vol. I. Aerodynamics. *Out of print.*
Vol. II. Seaplanes, Structures, Engines, Materials, etc. 40s (40s 8*d*.)

1935–36 Vol. I. Aerodynamics. 30s (30s. 7*d*.)
Vol. II. Structures, Flutter, Engines, Seaplanes, etc. 30s. (30s. 7*d*.)

1936 Vol. I. Aerodynamics General, Performance, Airscrews, Flutter and Spinning 40s. (40s. 9*d*.)
Vol. II. Stability and Control, Structures, Seaplanes, Engines, etc. 50s (50s. 10*d*.)

1937 Vol. I. Aerodynamics General, Performance, Airscrews, Flutter and Spinning. 40s. (40s. 10*d*.)
Vol. II. Stability and Control, Structures, Seaplanes, Engines, etc. 60s (61s.)

1938 Vol. I. Aerodynamics General, Performance, Airscrews. 50s (51s.)
Vol. II. Stability and Control, Flutter, Structures, Seaplanes, Wind Tunnels, Materials. 30s. (30s. 9*d*.)

1939 Vol. I. Aerodynamics General, Performance, Airscrews, Engines 50s. (50s. 11*d*.)
Vol. II. Stability and Control, Flutter and Vibration, Instruments, Structures, Seaplanes, etc. 63s. (64s. 2*d*.)

1940 Aero and Hydrodynamics, Aerofoils, Airscrews, Engines, Flutter, Icing, Stability and Control, Structures, and a miscellaneous section. 50s. (51s.)

Certain other reports proper to the 1940 volume will subsequently be included in a separate volume.

ANNUAL REPORTS OF THE AERONAUTICAL RESEARCH COUNCIL—

1933–34	1s. 6*d*. (1s. 8*d*.)
1934–35	1s. 6*d*. (1s. 8*d*.)
April 1, 1935 to December 31, 1936.	4s. (4s. 4*d*.)
1937	2s. (2s. 2*d*.)
1938	1s. 6*d*. (1s. 8*d*.)
1939–48	3s. (3s. 2*d*.)

INDEX TO ALL REPORTS AND MEMORANDA PUBLISHED IN THE ANNUAL TECHNICAL REPORTS, AND SEPARATELY—

April, 1950	R. & M. No 2600.	2s. 6*d*. (2s. 7½*d*.)

INDEXES TO THE TECHNICAL REPORTS OF THE AERONAUTICAL RESEARCH COUNCIL—

December 1, 1936 — June 30, 1939	R. & M. No. 1850.	1s. 3*d*. (1s. 4½*d*.)
July 1, 1939 — June 30, 1945.	R. & M. No. 1950.	1s. (1s. 1½*d*)
July 1, 1945 — June 30, 1946.	R. & M. No. 2050.	1s. (1s. 1½*d*)
July 1, 1946 — December 31, 1946	R. & M. No. 2150.	1s. 3*d*. (1s. 4½*d*.)
January 1, 1947 — June 30, 1947.	R. & M. No. 2250.	1s. 3*d* (1s. 4½*d*)

Prices in brackets include postage.

Obtainable from

HER MAJESTY'S STATIONERY OFFICE

York House Kingsway, LONDON, W.C.2 423 Oxford Street, LONDON, W.1
P.O Box 569, LONDON, S.E.1
13a Castle Street, EDINBURGH, 2 1 St. Andrew's Crescent, CARDIFF
39 King Street, MANCHESTER, 2 Tower Lane, BRISTOL, 1
2 Edmund Street, BIRMINGHAM, 3 80 Chichester Street, BELFAST

or through any bookseller.

S.O. Code No. 23–2559